

Experimental Validation of Cooperative RSS-based Localization with Unknown Transmit Power, Path Loss Exponent, and Precise Anchor Location

Yingquan Li, *Graduate Student Member, IEEE*, Bodhibrata Mukhopadhyay, *Member, IEEE*, Jiajie Xu, *Student Member, IEEE*, and Mohamed-Slim Alouini, *Fellow, IEEE*

Abstract—Received signal strength (RSS)–based cooperative localization has gained significant attention due to its straightforward system architectures and cost-effectiveness. In this paper, we propose Cooperative Localization Techniques (with Unknown Parameters), referred to as CTUP(s), which consider uncertainty in anchor nodes’ locations and assume the transmit power and path loss exponent (PLE) to be unknown. Unlike prior studies, CTUP(s) address unknowns by estimating these parameters, along with the location of target nodes. The non-convex and non-linear nature of the maximum likelihood (ML) estimator of the problem is addressed through relaxation techniques, employing Taylor series expansion, semidefinite relaxation (SDR), and the epigraph method. The resulting problem is solved using semidefinite second-order cone programming (SDP-SOCP), leveraging the precision of SDP and the simplicity of SOCP. We deployed an extensive network comprising 50 BLE nodes covering an area of 640 m × 180 m to gather RSS data. The precise location of the nodes is obtained using real-time kinematics global positioning system (RTK-GPS), which is treated as the ground truth. Furthermore, to replicate real-world scenarios, we recorded the positions of the anchor nodes using a standard GPS, thereby introducing uncertainty into the anchor node locations. Extensive simulation and hardware experimentation demonstrate the superior performance of CTUP compared to existing techniques.

Index Terms—Wireless sensor networks, cooperative localization, received signal strength (RSS), transmit power, path loss exponent (PLE).

I. INTRODUCTION

WIRELESS sensor networks (WSNs) have found extensive applications in diverse fields such as environmental monitoring, industrial management, smart cities, and healthcare [1]–[4]. Without the geographical location of the nodes, the sensing data lacks significance or context. In [5], the authors propose a framework for designing network localization and navigation (NLN) for the Internet of Things (IoT). However, equipping the nodes with a Global Positioning System (GPS) device is often impractical and cost-ineffective [6]. Additionally, GPS devices not only significantly impact nodes’ battery life due to high power consumption but also fail in

challenging operational environments, such as urban canyons and buildings [7]. Consequently, considerable research efforts are directed towards the development of efficient and precise localization techniques. Liu *et al.* [8] presents a localization system leveraging inertial measurements and spatial cooperation, featuring a graphical model for single-user and multi-user scenarios. In WSN, a subset of nodes, specifically a few, are presumed to have known locations and are identified as anchors. Leveraging these anchors, the locations of the remaining nodes, referred to as target nodes, are estimated or determined.

Localization techniques employ diverse measurements such as angle-of-arrival (AOA) [9], time-of-arrival (TOA) [10], time-difference-of-arrival (TDOA) [11], and received signal strength (RSS) [12] to estimate the location of target nodes. TOA and TDoA techniques stand out for their high accuracy in determining node positions. However, these techniques depend on precise clocks, which can pose significant challenges during real-world deployment, thereby presenting limited scalability in practical implementations. Furthermore, their dependence on sophisticated hardware and intricate signal processing algorithms adds complexity and cost to the system, potentially limiting their practicality in resource-constrained environments or large-scale deployments [13]. RSS-based localization determines node positions by analyzing the strength of the received signals from surrounding nodes [14]. This approach doesn’t necessitate precise time synchronization or specialized hardware, making it simpler to implement and more cost-effective. Therefore, RSS-based localization proves advantageous in scenarios where accuracy requirements are moderate and when hardware or synchronization constraints exist, making it suitable for localization in large networks [15].

RSS-based localization techniques determine the positions of target nodes using RSS values between anchor-target links and/or target-target links. The localization problem can broadly be solved using methods such as least squares (LS) [24] and maximum likelihood (ML) [25]. LS-based techniques are used for scenarios where the distribution of noise in RSS measurement is unknown. However, ML takes into account the noise statistics to achieve asymptotically optimal performance. Nevertheless, the ML is non-convex, non-linear, and has non-removable discontinuities, making it unsolvable using off-the-shelf techniques. Therefore, researchers have reformulated the ML problem into a tractable problem using various relaxation techniques [26]–[28].

Y. Li, J. Xu, and M. S. Alouini are with Computer, Electrical, and Mathematical Sciences and Engineering Division (CEMSE), King Abdullah University of Science and Technology (KAUST), Thuwal, 23955-6900, Kingdom of Saudi Arabia. Bodhibrata Mukhopadhyay was with CEMSE, KAUST, Thuwal, 23955-6900, Kingdom of Saudi Arabia. He is now with the department of Electronics and Communication, Indian Institute of Technology Roorkee, Uttarakhand, 247667, India (email: yingquan.li@kaust.edu.sa, bodhibrata@ece.iitr.ac.in, jiajie.xu.1@kaust.edu.sa, slim.alouini@kaust.edu.sa).

TABLE I
SUMMARY OF THE RSS-BASED LOCALIZATION TECHNIQUES. (NC: NON-COOPERATIVE, C: COOPERATIVE).

Algorithm	Unknown parameters	Estimated parameters			Manner	Method	Accuracy	Complexity	Year
		Location	Transmit power	PLE					
LSRE-Shi [16]	Transmit power	✓	✓	×	NC	SDP	Moderate	High	2020
RWLS-AE [17]	Transmit power & PLE	✓	✓	✓	NC	SDP	High	High	2021
SDP-Zou [18]	Transmit power & PLE Anchors' accurate location	✓	×	×	NC	SDP	Moderate	High	2021
RLBM [19]	Transmit power	✓	×	×	NC	SDP	Moderate	High	2021
MSL [20]	PLE	✓	×	✓	NC	LLS	Low	Low	2022
IRGDL [21]	None	✓	×	×	C	Invex Relaxation	High	Low	2022
SDP-I2 [22]	None	✓	×	×	C	SDP	High	High	2022
FCUP [23]	Transmit power	✓	✓	×	C	SDP-SOCP	High	Moderate	2023
CTUP-1	Anchors' accurate location	✓	×	×	C	SDP-SOCP	High	Moderate	2023
CTUP-2	PLE Anchors' accurate location		×	✓					
CTUP-3	Transmit power Anchors' accurate location		✓	×					
CTUP-4	Transmit power & PLE Anchors' accurate location		✓	✓					

In [29], the authors proposed a two-step linear least squares (LLS) estimator to obtain the location of the target nodes for a scenario where transmit power is unknown. In the first step, the authors obtained the ratio-of-distance estimates from the RSS measurement. Subsequently, they obtained the location by solving a set of linear equations. However, it has been observed that LLS demonstrates inadequate performance, particularly in scenarios with high levels of noise. To overcome the drawbacks of LLS, we explore non-linear least squares (NLS)-based methods.

In [27], the authors reformulated the ML optimization into a convex distributed problem, utilizing the alternating direction method of multipliers (ADMM). Then, they forced the solution towards the local minimum of the non-relaxed problem using soft transition. In [21], the authors relaxed the ML objective function into an invex optimization problem and solved it using gradient descent and coordinate descent. Researchers extensively used semidefinite programming (SDP) to solve the ML due to its guaranteed convergence and high accuracy [22], [30]. In [30], authors proposed a cooperative localization technique that first converts the log-normal shadowing RSS measurement model to a multiplicative model. Subsequently, the ML problem is reformulated into a non-convex estimator using relative error and finally solved using the semidefinite relaxation (SDR) technique. Wang *et al.* [22] addressed the localization problem for scenarios where RSS measurements are biased. They proposed two estimators using SDP with l_1 -norm and l_2 -norm, respectively. The above mentioned techniques require complete knowledge of transmit power, path loss exponent (PLE), and precise locations for anchor nodes.

The key model parameters of RSS-based localization techniques are the transmit power of the nodes, PLE, and anchor location uncertainty [31]¹. However, many studies assume extensive knowledge of these parameters, overlooking their susceptibility to various factors such as the battery level of the nodes [32], channel state [33], and antenna orienta-

tion [34]. The commonly used Log-normal model implies that the signal strength attenuation is caused by obstacles and diverse environmental conditions [35], posing challenges in accurately measuring transmit power. Additionally, PLE varies due to changes in transmitter frequency [36], weather patterns [37], and temperature fluctuations [38]. Studies have indicated that PLE is dynamic, typically ranging between 2 and 4 [39]–[41]. Generally, researchers use GPS to obtain the location of the anchor nodes; however, their measurement accuracy depends on several factors like satellite visibility, atmospheric conditions, and quality of the GPS module [42]. Moreover, in both maritime and aerial wireless networks, obtaining precise anchor locations (buoys in water and drones in the air) is hindered by factors like water currents and wind, respectively [43]. This proves the significance of incorporating uncertainty in anchor location as a model parameter. Researchers have designed and developed several non-cooperative localization (only using anchor-target links as measurement) techniques by assuming transmit power and (or) PLE to be unknown and (or) considering anchor location uncertainty. Shi *et al.* [16] utilized the least squares relative error (LSRE) to develop an estimator in the presence of unknown transmit power. The log-normal model was reformulated into a multiplicative form to facilitate semidefinite relaxation (SDR). In [20], the authors applied a weighted LLS framework to transform the ML estimator for unknown PLE scenarios. They proposed a bisection-based method to estimate the location of the target nodes. Zou *et al.* [18] used Taylor expansion and penalty factors to introduce a SDP-based estimator without knowing the transmit power and PLE. Then, the proposed estimator was extended for the scenarios with anchor location uncertainty. Sun *et al.* [17] introduced a method that alternately estimates unknown transmit power and PLE. Based on this, the authors presented two SDP-based estimators, each addressing one unknown parameter, and improved their efficacy using an iterative approach. Researchers deal with the unknown transmit power scenarios using RSS difference (RSSD)-based techniques. In [19], the authors proposed an iterative SDP-based technique by considering a mean squared error (MSE) minimization problem and finally transforming it into a convex

¹In this study, the transmit power of a node is defined as the power received from the node at a reference distance.

optimization problem using SDR. However, the aforementioned methods are exclusively applicable in non-cooperative localization. In Non-cooperative localization, each target node is required to solve one optimization problem, which leads to increased complexity, limited scalability, and increased power consumption. Unlike cooperative localization techniques [26], non-cooperative approaches face challenges in achieving high precision due to their inability to leverage target-target links.

There exist few cooperative localization techniques that incorporate both anchor-target links and target-target links, assuming certain model parameters to be unknown. In [23], the authors proposed a cooperative localization technique that jointly estimates the location and transmit power of target nodes. However, they assumed the PLE to be known and did not consider the anchor location uncertain. To address the above-mentioned issues, in this study, we propose SDP-SOCP-based cooperative localization techniques known as CTUP-1, CTUP-2, CTUP-3, and CTUP-4². These techniques aim to estimate the locations of target nodes across four distinct scenarios: i) transmit power and PLE are known, ii) PLE is unknown, iii) transmit power is unknown, and iv) both transmit power and PLE are unknown, respectively. We investigate the anchor-anchor wireless links to get an initial estimate of PLE as reported in [44]–[46]. In Table I, we provide a brief summary of the existing RSS-based localization techniques. Unlike our approach, none of the existing studies addressing anchor location uncertainty have conducted performance tests on real experimental data. The main contributions of this paper are summarized as follows:

- We proposed four cooperative techniques (CTUP-X) addressing scenarios dependent on the knowledge of transmit power and PLE, while also accounting for anchor location uncertainty. The proposed techniques can jointly estimate the location of target nodes, transmit power, and PLE depending on the scenarios.
- Cramer-Rao lower bound (CRLB) for RSS-based cooperative localization with unknown transmit power, PLE, and anchor location uncertainty.
- We created an indigenous dataset comprising RSS measurements between 50 nodes covering an area of 640 m × 180 m. The dataset also includes measurements of anchor uncertainty acquired through real-time kinematics (RTK) GPS and a standard GPS. To our knowledge, this is the most extensive and densely populated network utilized for localization.
- Extensive numerical simulations and real field experiments demonstrate the superior performance of CTUPs in terms of accuracy and computational complexity as compared to state-of-the-art techniques.

The rest of this paper is organized as follows. Section II presents the system model for RSS-based cooperative localization with anchor location uncertainty. Section III discusses the proposed SDP-SOCP-based estimators. The CRLB in the presence of unknown model parameters is derived in Section IV. Numerical results and experimental performance

TABLE II
TABLE OF NOTATIONS

Notations	Description
N_a	The number of anchor nodes
N_t	The number of target nodes
\mathbf{t}_j	The location of the j^{th} target node
$\check{\mathbf{s}}_i$	The location of the i^{th} anchor node
\mathbf{s}_i	The erroneous location of the i^{th} anchor node
\mathcal{T}	The index set for target nodes
\mathcal{A}	The index set for anchor nodes
$\bar{\mathcal{T}}_j$	The index set for the neighboring target nodes to \mathbf{t}_j
\mathcal{A}_j	The index set for the neighboring anchor nodes to \mathbf{t}_j
P_{ij}	The RSS measurement at $\check{\mathbf{s}}_i$ (or \mathbf{t}_i) when \mathbf{t}_j is the transmitter
P_j	The transmit power of \mathbf{t}_j
β	PLE
d_{ij}	The Euclidean distance between \mathbf{t}_j and $\check{\mathbf{s}}_i$ (or \mathbf{t}_i)
d_0	The reference distance
n_{ij}	The RSS measurement noise of P_{ij}
η_i	The anchor location uncertainty of \mathbf{s}_i
σ_{ij}	The standard deviation of n_{ij}
δ_i	The standard deviation of η_i
\mathbf{t}	The location of target nodes
$\check{\mathbf{s}}$	The location of anchor nodes
\mathbf{p}	The transmit power of target nodes
\mathbf{e}_j	The j^{th} column of $\mathbf{I}_{2(N_t+N_a)}$
\check{P}_{ij}	The RSS measurement at $\check{\mathbf{s}}_i$ when $\check{\mathbf{s}}_j$ is the transmitter
\check{P}_j	The transmit power of $\check{\mathbf{s}}_j$
\check{d}_{ij}	The Euclidean distance between \mathbf{s}_j and \mathbf{s}_i
$\check{\sigma}_{ij}$	The noise standard deviation of \check{P}_{ij}
β_0	The initial estimate of PLE
\mathcal{S}_j	The index set for the neighboring anchor nodes to \mathbf{s}_j
$ \mathcal{S} $	The number of anchor-anchor links
$ \mathcal{H} $	The number of target-anchor links and target-target links

are given in Section V. Finally, we conclude the paper in Section VI.

Notation: $|\mathcal{X}|$ denotes the cardinality of set \mathcal{X} . Vectors and matrices are represented by bold lowercase and bold uppercase letters, respectively. ℓ_2 -norm of a vector is given by $\|\cdot\|$. \mathbf{I}_N and $\mathbf{1}_N$ denote $N \times N$ identity matrix, and all-ones vectors with N rows respectively. $\mathbf{0}_{M,N}$ and $\mathbf{1}_{M,N}$ represent the all-zeros and all-ones matrices with M rows and N columns, respectively. $\mathbf{x}(m:n)$ represents the elements of \mathbf{x} from the m^{th} row to the n^{th} row. $\mathbf{X}_{m,n}$ represents the element of \mathbf{X} located at the intersection of the m^{th} row and the n^{th} column. $\mathbf{X}_{m:n,m:n}$ denotes a submatrix composed of rows m to n and columns m to n of \mathbf{X} . $\text{diag}(\mathbf{x})$ denotes the diagonal matrix with the elements of \mathbf{x} on the main diagonal. For a symmetric matrix \mathbf{X} , $\mathbf{X} \succcurlyeq \mathbf{0}$ implies that \mathbf{X} is positive semidefinite. $\text{tr}(\cdot)$ represents the trace of a matrix. $\text{Var}(\cdot)$ denotes the variance of a random variable. A summary of notations is presented in

²CTUP: Cooperative Technique with Unknown model Parameters

Table II.

II. SYSTEM MODEL

We consider a two-dimensional network consisting of N_a anchor nodes and N_t target nodes. The location of the j^{th} target node and the i^{th} anchor node are represented by \mathbf{t}_j and $\check{\mathbf{s}}_i$, respectively. We denote the set of indices of the target nodes and anchor nodes as \mathcal{T} and \mathcal{A} , respectively. A level of uncertainty in the positioning of the anchor nodes is taken into account. Based on the Log-normal signal propagation model [18], the received power and the erroneous anchor location are expressed using:

$$P_{ij} = P_j - 10\beta \log_{10} \frac{d_{ij}}{d_0} + n_{ij}, \quad j \in \mathcal{T}, \quad i \in \mathcal{A}_j \cup \mathcal{T}_j, \quad (1a)$$

$$\mathbf{s}_i = \check{\mathbf{s}}_i + \eta_i \mathbf{1}_2, \quad i \in \mathcal{A}, \quad (1b)$$

where P_{ij} is the received power at $\check{\mathbf{s}}_i$ (or \mathbf{t}_i) when \mathbf{t}_j is transmitting. The Euclidian distance between two nodes are given by $d_{ij} = \|\mathbf{t}_j - \check{\mathbf{s}}_i\|$ (or $\|\mathbf{t}_j - \mathbf{t}_i\|$). The reference distance d_0 is considered to be 1 m. P_j is the received power at d_0 and will be referred to as the transmit power of \mathbf{t}_j , and β is PLE. The neighboring target nodes and anchor nodes of \mathbf{t}_j are indexed by \mathcal{T}_j and \mathcal{A}_j , respectively. The RSS measurement noise (n_{ij}) and anchor location uncertainty (η_i) are assumed to follow Gaussian distribution and are represented as $n_{ij} \sim \mathcal{N}(0, \sigma_{ij}^2)$ and $\eta_i \sim \mathcal{N}(0, \delta_i^2)$, respectively. We assume the components of \mathbf{s}_i are independent random variables. Let $\mathbf{t} = [\mathbf{t}_1^T, \dots, \mathbf{t}_{N_t}^T]^T$ and $\mathbf{p} = [P_1, \dots, P_{N_t}]^T$ be the location and transmit power of the target nodes, respectively. We define the precise location of anchor nodes as $\check{\mathbf{s}} = [\check{\mathbf{s}}_1^T, \dots, \check{\mathbf{s}}_{N_a}^T]^T$. Let $\boldsymbol{\theta} = [\mathbf{t}^T, \check{\mathbf{s}}^T, \mathbf{p}^T, \beta]^T$ be the unknown parameter vector and $\mathbf{m} = [\dots, P_{ij}, \dots, \mathbf{s}_1^T, \dots, \mathbf{s}_{N_a}^T]^T$ be the collection of RSS and anchor location measurements. The probability density function (PDF) of \mathbf{m} given $\boldsymbol{\theta}$ is expressed as $p(\mathbf{m}; \boldsymbol{\theta}) =$

$$\prod_{\substack{j \in \mathcal{T} \\ i \in \mathcal{A}_j \cup \mathcal{T}_j}} \frac{1}{\sqrt{2\pi\sigma_{ij}^2}} \exp \left[\frac{(P_{ij} - P_j + 10\beta \log_{10} d_{ij})^2}{-2\sigma_{ij}^2} \right] \times \prod_{i \in \mathcal{A}} \frac{1}{\sqrt{2\pi\delta_i^2}} \exp \left[\frac{\|\mathbf{s}_i - \check{\mathbf{s}}_i\|^2}{-2\delta_i^2} \right]. \quad (2)$$

The ML estimator for $\boldsymbol{\theta}$ is given by using (2) [47]

$$\min_{\boldsymbol{\theta}} \sum_{\substack{j \in \mathcal{T} \\ i \in \mathcal{A}_j \cup \mathcal{T}_j}} \sigma_{ij}^{-2} (P_{ij} - P_j + 10\beta \log_{10} d_{ij})^2 + \sum_{i \in \mathcal{A}} \delta_i^{-2} \|\mathbf{s}_i - \check{\mathbf{s}}_i\|^2. \quad (3)$$

III. COOPERATIVE LOCALIZATION ALGORITHMS

A. Scenario I: Transmit power and PLE are known

In the first scenario, we assume that both the transmit power of target nodes and PLE are known. Through the utilization of Taylor expansion for n_{ij} , (1a) can be reformulated as

$$d_{ij}^2 = 10^{\frac{P_j - P_{ij}}{5\beta}} 10^{\frac{n_{ij}}{5\beta}} \approx 10^{\frac{P_j - P_{ij}}{5\beta}} \left(1 + \frac{\ln 10}{5\beta} n_{ij} \right) = 10^{\frac{P_j - P_{ij}}{5\beta}} + \zeta_{ij}, \quad (4)$$

where $\zeta_{ij} \sim \mathcal{N} \left(0, \left(10^{\frac{P_j - P_{ij}}{5\beta}} \frac{\ln 10}{5\beta} \sigma_{ij} \right)^2 \right)$. Now, let $\boldsymbol{\mu} = [\mathbf{t}^T, \check{\mathbf{s}}^T]^T$ be a vector representing the location of the target nodes and anchor nodes. The PDF of \mathbf{m} can be expressed as $p(\mathbf{m}; \boldsymbol{\mu}) =$

$$\prod_{\substack{j \in \mathcal{T} \\ i \in \mathcal{A}_j \cup \mathcal{T}_j}} \frac{1}{\sqrt{2\pi\tilde{\zeta}_{ij}^2}} \exp \left[\frac{\left(d_{ij}^2 - 10^{\frac{P_j - P_{ij}}{5\beta}} \right)^2}{-2\tilde{\zeta}_{ij}^2} \right] \times \prod_{i \in \mathcal{A}} \frac{1}{\sqrt{2\pi\delta_i^2}} \exp \left[\frac{\|\mathbf{s}_i - \check{\mathbf{s}}_i\|^2}{-2\delta_i^2} \right], \quad (5)$$

where $\tilde{\zeta}_{ij} = 10^{\frac{P_j - P_{ij}}{5\beta}} \frac{\ln 10}{5\beta} \sigma_{ij}$. The ML estimator for \mathbf{t} is given by

$$\min_{\boldsymbol{\mu}} \sum_{\substack{j \in \mathcal{T} \\ i \in \mathcal{A}_j \cup \mathcal{T}_j}} \left(\frac{d_{ij}^2 - 10^{\frac{P_j - P_{ij}}{5\beta}}}{\tilde{\zeta}_{ij}} \right)^2 + \sum_{i \in \mathcal{A}} \frac{\|\mathbf{s}_i - \check{\mathbf{s}}_i\|^2}{\delta_i^2} \quad (6a)$$

$$\text{s.t. } d_{ij} = \|\mathbf{t}_j - \check{\mathbf{s}}_i\|, \quad j \in \mathcal{T}, \quad i \in \mathcal{A}_j, \quad (6b)$$

$$d_{ij} = \|\mathbf{t}_j - \mathbf{t}_i\|, \quad j \in \mathcal{T}, \quad i \in \mathcal{T}_j. \quad (6c)$$

The optimization problem in (6) is non-convex and can not be solved using standard techniques. To mitigate the non-convexity resulting from the norm constraint, we firstly square both sides of (6b) and (6c) to reformulate (6) as

$$\min_{\boldsymbol{\mu}} \sum_{\substack{j \in \mathcal{T} \\ i \in \mathcal{A}_j \cup \mathcal{T}_j}} \left(\frac{d_{ij}^2 - 10^{\frac{P_j - P_{ij}}{5\beta}}}{\tilde{\zeta}_{ij}} \right)^2 + \sum_{i \in \mathcal{A}} \frac{\|\mathbf{s}_i - \check{\mathbf{s}}_i\|^2}{\delta_i^2} \quad (7a)$$

$$\text{s.t. } d_{ij}^2 = \|\mathbf{t}_j - \check{\mathbf{s}}_i\|^2, \quad j \in \mathcal{T}, \quad i \in \mathcal{A}_j, \quad (7b)$$

$$d_{ij}^2 = \|\mathbf{t}_j - \mathbf{t}_i\|^2, \quad j \in \mathcal{T}, \quad i \in \mathcal{T}_j. \quad (7c)$$

Subsequently, we introduce an auxiliary variable $\mathbf{K} = \boldsymbol{\mu}\boldsymbol{\mu}^T$ to represent d_{ij}^2 in a manner satisfying the requirements of SDP. Likewise, $\|\mathbf{s}_i - \check{\mathbf{s}}_i\|^2$ can also be rewritten in a similar format. Consequently, we can rewrite (7) as

$$\min_{u_{ij}, \lambda_i, \boldsymbol{\mu}, \mathbf{K}} \sum_{\substack{j \in \mathcal{T} \\ i \in \mathcal{A}_j \cup \mathcal{T}_j}} \left(\frac{u_{ij} - 10^{\frac{P_j - P_{ij}}{5\beta}}}{\tilde{\zeta}_{ij}} \right)^2 + \sum_{i \in \mathcal{A}} \delta_i^{-2} \lambda_i \quad (8a)$$

$$\text{s.t. } u_{ij} = \text{tr}(\boldsymbol{\Xi}_j \mathbf{K} \boldsymbol{\Xi}_j^T - 2\boldsymbol{\Xi}_j \mathbf{K} \boldsymbol{\Psi}_i^T + \boldsymbol{\Psi}_i \mathbf{K} \boldsymbol{\Psi}_i^T), \quad j \in \mathcal{T}, \quad i \in \mathcal{A}_j, \quad (8b)$$

$$u_{ij} = \text{tr}(\boldsymbol{\Xi}_j \mathbf{K} \boldsymbol{\Xi}_j^T - 2\boldsymbol{\Xi}_j \mathbf{K} \boldsymbol{\Xi}_i^T + \boldsymbol{\Xi}_i \mathbf{K} \boldsymbol{\Xi}_i^T), \quad j \in \mathcal{T}, \quad i \in \mathcal{T}_j, \quad (8c)$$

$$\lambda_i = \text{tr}(\boldsymbol{\Psi}_i \mathbf{K} \boldsymbol{\Psi}_i^T) - 2\mathbf{s}_i^T \boldsymbol{\Psi}_i \boldsymbol{\mu} + \|\mathbf{s}_i\|^2, \quad i \in \mathcal{A}, \quad (8d)$$

$$\mathbf{K} = \boldsymbol{\mu}\boldsymbol{\mu}^T, \quad (8e)$$

$$\text{rank}(\mathbf{K}) = 1, \quad (8f)$$

where $\boldsymbol{\Xi}_i = [\mathbf{e}_{2i-1}, \mathbf{e}_{2i}]^T$ and $\boldsymbol{\Psi}_i = [\mathbf{e}_{2i+2N_t-1}, \mathbf{e}_{2i+2N_t}]^T$, \mathbf{e}_j is the j^{th} column of $\mathbf{I}_{2(N_t+N_a)}$. In (8), u_{ij} and λ_i are auxiliary variables representing d_{ij}^2 and $\|\mathbf{s}_i - \check{\mathbf{s}}_i\|^2$, respectively.

By dropping off the rank constraint and relaxing (8e), an estimator based on SDP can be obtained

$$\min_{u_{ij}, \lambda_i, \boldsymbol{\mu}, \mathbf{K}} \sum_{\substack{j \in \mathcal{T} \\ i \in \mathcal{A}_j \cup \mathcal{T}_j}} \left(\frac{u_{ij} - 10^{\frac{P_j - P_{ij}}{5\beta}}}{\tilde{\zeta}_{ij}} \right)^2 + \sum_{i \in \mathcal{A}} \delta_i^{-2} \lambda_i \quad (9a)$$

$$\text{s.t.} \quad (8b), (8c), (8d), \quad (9b)$$

$$\begin{bmatrix} 1 & \boldsymbol{\mu}^T \\ \boldsymbol{\mu} & \mathbf{K} \end{bmatrix} \succeq \mathbf{0}.$$

The location of target nodes can be estimated by using interior point methods to solve (9) [48], [49]. However, SDP-based estimator has higher computational complexity than those based on SOCP. Exploiting the low complexity of SOCP, we rewrite (9) as an epigraph form using the auxiliary variable ω

$$\min_{\substack{u_{ij}, \lambda_i, \boldsymbol{\mu}, \\ \mathbf{K}, \omega}} \omega + \sum_{i \in \mathcal{A}} \delta_i^{-2} \lambda_i \quad (10a)$$

$$\text{s.t.} \quad \sum_{\substack{j \in \mathcal{T} \\ i \in \mathcal{A}_j \cup \mathcal{T}_j}} \tilde{\zeta}_{ij}^{-2} \left(u_{ij} - 10^{\frac{P_j - P_{ij}}{5\beta}} \right)^2 \leq \omega, \quad (10b)$$

(8b), (8c), (8d), (9b).

The optimization problem (10) is not a SOCP as the constraint (10b) is not a linear matrix inequality form. To address this issue, we use an auxiliary variable $\boldsymbol{\xi} = [\dots, \xi_{ij}, \dots]$ and reformulate (9) into a mixed SDP-SOCP problem.

$$\min_{\substack{u_{ij}, \lambda_i, \boldsymbol{\mu}, \\ \mathbf{K}, \omega, \boldsymbol{\xi}}} \omega + \sum_{i \in \mathcal{A}} \delta_i^{-2} \lambda_i \quad (11a)$$

$$\text{s.t.} \quad \|[2\boldsymbol{\xi}^T, \omega - 1]\| \leq \omega + 1, \quad (11b)$$

$$\text{diag}([\dots, \xi_{ij} - \tilde{\zeta}_{ij}^{-1} \left(u_{ij} - 10^{\frac{P_j - P_{ij}}{5\beta}} \right), \dots, \\ \dots, -\xi_{ij} + \tilde{\zeta}_{ij}^{-1} \left(u_{ij} - 10^{\frac{P_j - P_{ij}}{5\beta}} \right), \dots]) \succeq \mathbf{0},$$

$$j \in \mathcal{T}, i \in \mathcal{A}_j \cup \mathcal{T}_j, \quad (11c)$$

(8b), (8c), (8d), (9b).

The proposed estimator in (11) benefits from the high accuracy of SDP and low complexity of SOCP, which is referred to as CTUP-1. The estimated location of the target nodes is obtained using $\hat{\mathbf{t}}_j = \hat{\boldsymbol{\mu}}(2j - 1 : 2j)^T$.

B. Scenario II: PLE is unknown

In this scenario, we consider β to be unknown. The anchor nodes communicating with $\check{s}_j (j \in \mathcal{A})$ are indexed by \mathcal{S}_j . The total number of available links in a network is given by $|\mathcal{S}| = \sum_j |\mathcal{S}_j|$. The RSS measurement and the Euclidean distance between the anchor nodes $\check{s}_j (j \in \mathcal{A})$ and $\check{s}_i (i \in \mathcal{S}_j)$ are represented by \check{P}_{ij} and \check{d}_{ij} , respectively. The transmit power of \check{s}_j , represented by \check{P}_j , is assumed to be known. The RSS measurements are affected by additive zero-mean Gaussian noise, which is characterized by $\mathcal{N}(0, \check{\sigma}_{ij}^2)$. By letting $\check{\mathbf{m}} = [\dots, \check{P}_{ij}, \dots]^T$ be the collection of RSS measurements,

the conditional joint PDF of $\check{\mathbf{m}}$ given PLE is expressed as $p(\check{\mathbf{m}}; \beta) =$

$$\prod_{\substack{j \in \mathcal{A} \\ i \in \mathcal{S}_j}} \frac{1}{\sqrt{2\pi\check{\sigma}_{ij}^2}} \exp \left[\frac{\left(\check{P}_{ij} - \check{P}_j + 10\beta \log_{10} \check{d}_{ij} \right)^2}{-2\check{\sigma}_{ij}^2} \right]. \quad (12)$$

Thus, the ML estimator of β obtained using (12) is given by

$$\min_{\beta} \sum_{\substack{j \in \mathcal{A} \\ i \in \mathcal{S}_j}} \check{\sigma}_{ij}^{-2} \left(\check{P}_{ij} - \check{P}_j + 10\beta \log_{10} \check{d}_{ij} \right)^2. \quad (13)$$

The objective function is convex with respect to β and achieves the global minimum (β_0) at its stationary point. An initial estimate of β is expressed as

$$\beta_0 = \frac{\mathbf{1}_{|\mathcal{S}|}^T \check{\mathbf{Q}} \check{\mathbf{q}}}{\mathbf{1}_{|\mathcal{S}|}^T \check{\mathbf{Q}} \check{\boldsymbol{\phi}}}, \quad (14)$$

where $\check{\mathbf{Q}} = \text{diag}([\dots, \check{\sigma}_{ij}^{-2}, \dots])$, $\check{\mathbf{q}} = [\dots, \check{P}_j - \check{P}_{ij}, \dots]^T$ and $\check{\boldsymbol{\phi}} = [\dots, 10 \log_{10} \check{d}_{ij}, \dots]^T$, $j \in \mathcal{A}$, $i \in \mathcal{S}_j$.

We express $\beta = \beta_0(1 + \epsilon)$ where $\epsilon = \frac{\beta - \beta_0}{\beta_0}$. When β_0 is sufficiently close to β , (1a) can be reformulated into

$$d_{ij}^2 = 10^{\frac{P_j - P_{ij}}{5\beta_0(1+\epsilon)}} 10^{\frac{n_{ij}}{5\beta}} \approx 10^{\frac{P_j - P_{ij}}{5\beta_0}(1-\epsilon)} \left(1 + \frac{\ln 10}{5\beta_0} n_{ij} \right). \quad (15)$$

Applying Taylor expansion into (15) yields

$$d_{ij}^2 \approx 10^{\frac{P_j - P_{ij}}{5\beta_0}} - 10^{\frac{P_j - P_{ij}}{5\beta_0}} \frac{(P_j - P_{ij}) \epsilon \ln 10}{5\beta_0} + \tau_{ij}, \quad (16)$$

where $\tau_{ij} \sim \mathcal{N}(0, \tilde{\tau}_{ij}^2)$ and $\tilde{\tau}_{ij}$ is expressed as

$$\tilde{\tau}_{ij} = 10^{\frac{P_j - P_{ij}}{5\beta_0}} \left(1 - \frac{(P_j - P_{ij}) \epsilon \ln 10}{5\beta_0} \right) \frac{\ln 10}{5\beta_0} \sigma_{ij}$$

$$\approx 10^{\frac{P_j - P_{ij}}{5\beta_0}} \frac{\ln 10}{5\beta_0} \sigma_{ij}. \quad (17)$$

By letting $\chi_{ij} = 10^{\frac{P_j - P_{ij}}{5\beta_0}} \frac{(P_j - P_{ij}) \ln 10}{5\beta_0}$, the ML estimator for \mathbf{t} and β is formulated using (16) as

$$\min_{\boldsymbol{\mu}, \epsilon} \sum_{\substack{j \in \mathcal{T} \\ i \in \mathcal{A}_j \cup \mathcal{T}_j}} \tilde{\tau}_{ij}^{-2} \left(d_{ij}^2 - 10^{\frac{P_j - P_{ij}}{5\beta_0}} + \chi_{ij} \epsilon \right)^2$$

$$+ \sum_{i \in \mathcal{A}} \delta_i^{-2} \|\mathbf{s}_i - \check{\mathbf{s}}_i\|^2 \quad (18a)$$

$$\text{s.t.} \quad d_{ij} = \|\mathbf{t}_j - \check{\mathbf{s}}_i\|, \quad j \in \mathcal{T}, i \in \mathcal{A}_j, \quad (18b)$$

$$d_{ij} = \|\mathbf{t}_j - \mathbf{t}_i\|, \quad j \in \mathcal{T}, i \in \mathcal{T}_j. \quad (18c)$$

Following the approach used in (9), the minimization problem can be transformed through SDR

$$\min_{\substack{u_{ij}, \lambda_i, \boldsymbol{\mu}, \\ \mathbf{K}, \epsilon}} \underbrace{\sum_{\substack{j \in \mathcal{T} \\ i \in \mathcal{A}_j \cup \mathcal{T}_j}} \tilde{\tau}_{ij}^{-2} \left(u_{ij} - 10^{\frac{P_j - P_{ij}}{5\beta_0}} + \chi_{ij} \epsilon \right)^2}_z$$

$$+ \sum_{i \in \mathcal{A}} \delta_i^{-2} \lambda_i \quad (19a)$$

$$\text{s.t.} \quad (8b), (8c), (8d), (9b).$$

The objective function of (19) can be converted into a linear form by considering the epigraph of z using an auxiliary variable ω . Also, with the assistance of another auxiliary variable $\boldsymbol{\xi} = [\dots, \xi_{ij}, \dots]$, we convert the epigraph constraint ($z \leq \omega$) to an LMI constraint and finally represent (19) into an SDP-SOCP formulation

$$\min_{\substack{u_{ij}, \lambda_i, \mu, \\ \mathbf{K}, \epsilon, \omega, \boldsymbol{\xi}}} \omega + \sum_{i \in \mathcal{A}} \delta_i^{-2} \lambda_i \quad (20a)$$

$$\text{s.t.} \quad \|[2\boldsymbol{\xi}^T, \omega - 1]\| \leq \omega + 1, \quad (20b)$$

$$\text{diag}\left([\dots, \xi_{ij} - \left(\frac{u_{ij} - 10^{\frac{P_j - P_{ij}}{5\beta_0}} + \chi_{ij}\epsilon}{\tilde{r}_{ij}}\right), \dots, \dots, -\xi_{ij} + \left(\frac{u_{ij} - 10^{\frac{P_j - P_{ij}}{5\beta_0}} + \chi_{ij}\epsilon}{\tilde{r}_{ij}}\right), \dots]\right) \succcurlyeq \mathbf{0},$$

$$j \in \mathcal{T}, i \in \mathcal{A}_j \cup \mathcal{T}_j, \quad (20c)$$

$$(8b), (8c), (8d), (9b).$$

Solving (20), we get an estimate of \mathbf{t} and β via $\hat{\mathbf{t}}_j = \hat{\boldsymbol{\mu}}(2j - 1 : 2j)^T$ and $\hat{\beta} = \beta_0(1 + \hat{\epsilon})$, respectively, and we refer to it as CTUP-2.

C. Scenario III: Transmit power is unknown

In this section, the transmit power is unknown and is jointly estimated along with the location of target nodes. By rearranging the terms of (1a), we have

$$d_{ij}^2 10^{\frac{P_{ij}}{5\beta}} = 10^{\frac{P_j}{5\beta}} 10^{\frac{n_{ij}}{5\beta}} \approx 10^{\frac{P_j}{5\beta}} \left(1 + \frac{\ln 10}{5\beta} n_{ij}\right) = 10^{\frac{P_j}{5\beta}} + \rho_{ij}, \quad (21)$$

where $\rho_{ij} \sim \mathcal{N}\left(0, \left(10^{\frac{P_j}{5\beta}} \frac{\ln 10}{5\beta} = \tilde{\rho}_{ij}\right)^2\right)$. Unlike in Section III-A and Section III-B, it is not possible to estimate \mathbf{t} and \mathbf{p} by solving the ML estimator obtained from (21) as $\tilde{\rho}_{ij}$ is unknown. Thus, in this scenario, we employ the NLS estimator, a commonly used technique known for its verified effectiveness, especially in cases involving unknown noise statistics. [14], [47]. Therefore, we reformulate (21) as an NLS optimization problem aiming to minimize the sum of squared errors

$$\min_{\boldsymbol{\mu}, \mathbf{p}} \sum_{\substack{j \in \mathcal{T} \\ i \in \mathcal{A}_j \cup \mathcal{T}_j}} \left(d_{ij}^2 10^{\frac{P_{ij}}{5\beta}} - 10^{\frac{P_j}{5\beta}}\right)^2 + \sum_{i \in \mathcal{A}} \|\mathbf{s}_i - \check{\mathbf{s}}_i\|^2 \quad (22a)$$

$$\text{s.t.} \quad d_{ij} = \|\mathbf{t}_j - \check{\mathbf{s}}_i\|, \quad j \in \mathcal{T}, i \in \mathcal{A}_j, \quad (22b)$$

$$d_{ij} = \|\mathbf{t}_j - \mathbf{t}_i\|, \quad j \in \mathcal{T}, i \in \mathcal{T}_j. \quad (22c)$$

The non-convex constraints in (22) are convexified through the utilization of auxiliary variables $\mathbf{K} = \boldsymbol{\mu}\boldsymbol{\mu}^T$ and $\lambda_i = \|\mathbf{s}_i - \check{\mathbf{s}}_i\|^2$. By considering $g_j = 10^{\frac{P_j}{5\beta}}$ and $u_{ij} = d_{ij}^2$ we can express (22) as

$$\min_{\substack{u_{ij}, g_j, \lambda_i, \\ \boldsymbol{\mu}, \mathbf{K}}} \sum_{\substack{j \in \mathcal{T} \\ i \in \mathcal{A}_j \cup \mathcal{T}_j}} \left(u_{ij} 10^{\frac{P_{ij}}{5\beta}} - g_j\right)^2 + \sum_{i \in \mathcal{A}} \lambda_i \quad (23a)$$

$$\text{s.t.} \quad (8b), (8c), (8d), (9b).$$

We introduce an epigraph variable ω for the first term of (23a) and an auxiliary variables $\boldsymbol{\xi}$ to obtain the LMI constraint. Thus, we convert the SDP in (23) to an SDP-SOCP problem.

$$\min_{\substack{u_{ij}, g_j, \lambda_i, \\ \boldsymbol{\mu}, \mathbf{K}, \omega, \boldsymbol{\xi}}} \omega + \sum_{i \in \mathcal{A}} \lambda_i \quad (24a)$$

$$\text{s.t.} \quad \|[2\boldsymbol{\xi}^T, \omega - 1]\| \leq \omega + 1, \quad (24b)$$

$$\text{diag}\left([\dots, \xi_{ij} - u_{ij} 10^{\frac{P_{ij}}{5\beta}} + g_j, \dots, \dots, -\xi_{ij} + u_{ij} 10^{\frac{P_{ij}}{5\beta}} - g_j, \dots]\right) \succcurlyeq \mathbf{0},$$

$$j \in \mathcal{T}, i \in \mathcal{A}_j \cup \mathcal{T}_j, \quad (24c)$$

$$(8b), (8c), (8d), (9b).$$

By solving (24), we can obtain the location and transmit power of target nodes using $\hat{\mathbf{t}}_j = \hat{\boldsymbol{\mu}}(2j - 1 : 2j)^T$ and $\hat{P}_j = 5\beta \log_{10} \hat{g}_j$. We refer to the technique as CTUP-3.

D. Scenario IV: Transmit power and PLE are unknown

As the transmit power and PLE are unknown, we rewrite (1a) as a multiplicative form and square both side

$$d_{ij}^2 10^{\frac{P_{ij}}{5\beta}} = 10^{\frac{P_j}{5\beta_0(1+\epsilon)}} 10^{\frac{n_{ij}}{5\beta}} \approx 10^{\frac{P_j}{5\beta_0}(1-\epsilon)} 10^{\frac{n_{ij}}{5\beta}}, \quad (25)$$

where ϵ is defined in Section III-B. By performing Taylor expansion at $\epsilon = 0$ with sufficiently small noise, (25) is reformulated into

$$d_{ij}^2 10^{\frac{P_{ij}}{5\beta_0}} \approx 10^{\frac{P_j}{5\beta_0}} \left(1 - \frac{P_j \epsilon \ln 10}{5\beta_0}\right) \left(1 + \frac{\ln 10}{5\beta} n_{ij}\right) = 10^{\frac{P_j}{5\beta_0}} - 10^{\frac{P_j}{5\beta_0}} \frac{P_j \epsilon \ln 10}{5\beta_0} + \nu_{ij}, \quad (26)$$

where ν_{ij} is a zero-mean Gaussian random variable with its unknown standard deviation given by

$$\tilde{\nu}_{ij} = 10^{\frac{P_j}{5\beta_0}} \left(1 - \frac{P_j \epsilon \ln 10}{5\beta_0}\right) \frac{\ln 10}{5\beta} \sigma_{ij}. \quad (27)$$

Similar to the method in Section III-C, the NLS estimator is given by

$$\min_{\boldsymbol{\mu}, \mathbf{p}, \beta} \sum_{\substack{j \in \mathcal{T} \\ i \in \mathcal{A}_j \cup \mathcal{T}_j}} \left(d_{ij}^2 10^{\frac{P_{ij}}{5\beta_0}} - 10^{\frac{P_j}{5\beta_0}} + 10^{\frac{P_j}{5\beta_0}} \frac{P_j \epsilon \ln 10}{5\beta_0}\right)^2 + \sum_{i \in \mathcal{A}} \|\mathbf{s}_i - \check{\mathbf{s}}_i\|^2 \quad (28a)$$

$$\text{s.t.} \quad d_{ij} = \|\mathbf{t}_j - \check{\mathbf{s}}_i\|, \quad j \in \mathcal{T}, i \in \mathcal{A}_j, \quad (28b)$$

$$d_{ij} = \|\mathbf{t}_j - \mathbf{t}_i\|, \quad j \in \mathcal{T}, i \in \mathcal{T}_j. \quad (28c)$$

The auxiliary variables \mathbf{K} and λ_i are used to tackle the non-convexity of (28). By defining $g_j = 10^{\frac{P_j}{5\beta_0}}$ and $r_j = 10^{\frac{P_j}{5\beta_0}} \frac{P_j \epsilon \ln 10}{5\beta_0}$, we obtain the following optimization problem

$$\min_{\substack{u_{ij}, g_j, r_j, \\ \lambda_i, \boldsymbol{\mu}, \mathbf{K}}} \sum_{\substack{j \in \mathcal{T} \\ i \in \mathcal{A}_j \cup \mathcal{T}_j}} \left(10^{\frac{P_{ij}}{5\beta_0}} u_{ij} - g_j + r_j\right)^2 + \sum_{i \in \mathcal{A}} \lambda_i \quad (29a)$$

$$\text{s.t.} \quad (8b), (8c), (8d), (9b).$$

The optimization problem (29) can be solved by standard SDP solvers, which have high computational complexity. To address

Algorithm 1 CTUP-4: The cooperative technique with unknown transmit power and PLE

Input: $N_a, N_t, \mathcal{A}_j, \mathcal{T}_j, \mathcal{S}_j, \mathbf{m}, \check{\mathbf{Q}}, \check{\mathbf{q}}, \check{\phi}, \mathbf{Q}$.

- 1: Compute β_0 using (14).
- 2: Solve the SDP-SOCP problem in (31) to obtain $\hat{\mathbf{t}}_j = \hat{\boldsymbol{\mu}}(2j-1:2j)^T$ and $\hat{d}_{ij} = \sqrt{\hat{u}_{ij}}, j \in \mathcal{T}, i \in \mathcal{A}_j \cup \mathcal{T}_j$.
- 3: Compute $\mathbf{h}_j = P_{ij} + 10\beta_0 \log_{10} \hat{d}_{ij}, j \in \mathcal{T}, i \in \mathcal{A}_j \cup \mathcal{T}_j$.
- 4: Compute \hat{P}_j using (32a), $j \in \mathcal{T}$.
- 5: Compute $q_{ij} = \hat{P}_j - P_{ij}$ and $\phi_{ij} = 10 \log_{10} \hat{d}_{ij}, j \in \mathcal{T}, i \in \mathcal{A}_j \cup \mathcal{T}_j$. \mathbf{q} comprises all q_{ij} , and ϕ comprises all ϕ_{ij} .

- 6: Compute $\hat{\beta}$ using (32b).

Output: $\hat{\mathbf{t}}_j, \hat{P}_j, \hat{\beta}, j \in \mathcal{T}$.

this issue, the objective function is converted to the epigraph form by applying an auxiliary variable ω

$$\min_{\substack{u_{ij}, g_j, r_j, \\ \lambda_i, \mu, \mathbf{K}, \omega}} \omega + \sum_{i \in \mathcal{A}} \lambda_i \quad (30a)$$

$$\text{s.t.} \quad \sum_{\substack{j \in \mathcal{T} \\ i \in \mathcal{A}_j \cup \mathcal{T}_j}} \left(10^{\frac{P_{ij}}{5\beta_0}} u_{ij} - g_j + r_j \right)^2 \leq \omega, \quad (30b)$$

(8b), (8c), (8d), (9b).

To convert (30) into an SDP-SOCP problem, we introduce $\boldsymbol{\xi}$ which stacks all values $\xi_{ij} = u_{ij} 10^{\frac{P_{ij}}{5\beta_0}} - g_j + r_j, j \in \mathcal{T}, i \in \mathcal{A}_j \cup \mathcal{T}_j$ to obtain an LMI

$$\min_{\substack{u_{ij}, g_j, r_j, \\ \lambda_i, \mu, \mathbf{K}, \omega, \boldsymbol{\xi}}} \omega + \sum_{i \in \mathcal{A}} \lambda_i \quad (31a)$$

$$\text{s.t.} \quad \left\| [2\boldsymbol{\xi}^T, \omega - 1] \right\| \leq \omega + 1, \quad (31b)$$

$$\text{diag}([\dots, \xi_{ij} - 10^{\frac{P_{ij}}{5\beta_0}} u_{ij} + g_j - r_j, \dots, \\ \dots, -\xi_{ij} + 10^{\frac{P_{ij}}{5\beta_0}} u_{ij} - g_j + r_j, \dots]) \succeq \mathbf{0}, \\ j \in \mathcal{T}, i \in \mathcal{A}_j \cup \mathcal{T}_j, \quad (31c)$$

(8b), (8c), (8d), (9b).

The proposed estimator in (31) can obtain the location of target nodes (\mathbf{t}), their transmit powers (\mathbf{p}), and β . However, the estimated accuracy of \mathbf{p} and β is poor. We obtain a better estimate of \mathbf{p} and β by exploiting the fact that (3) is a convex function with respect to \mathbf{p} and β , respectively

$$\hat{P}_j = \frac{\mathbf{1}_{|\mathcal{A}_j \cup \mathcal{T}_j|}^T \mathbf{Q} \mathbf{h}_j}{\mathbf{1}_{|\mathcal{A}_j \cup \mathcal{T}_j|}^T \mathbf{Q} \mathbf{1}_{|\mathcal{A}_j \cup \mathcal{T}_j|}}, \quad (32a)$$

$$\hat{\beta} = \frac{\mathbf{1}_{|\mathcal{H}|}^T \mathbf{Q} \mathbf{q}}{\mathbf{1}_{|\mathcal{H}|}^T \mathbf{Q} \phi}, \quad (32b)$$

where \mathbf{Q} is the covariance matrix of n_{ij} , \mathbf{h}_j stacks $P_{ij} + 10\beta \log_{10} d_{ij}$, \mathbf{q} stacks $P_j - P_{ij}$, and ϕ stacks $10 \log_{10} d_{ij}, j \in \mathcal{T}, i \in \mathcal{A}_j \cup \mathcal{T}_j$. The total number of anchor-target links and target-target links are expressed as $|\mathcal{H}| = \sum_j |\mathcal{A}_j \cup \mathcal{T}_j|$. In Algorithm 1, we summarize The proposed technique dealing with the scenario for unknown transmit power and PLE. We refer to it as CTUP-4.

IV. CRAMER-RAO LOWER BOUNDS (CRLB)

The CRLB provides a theoretical lower bound for unbiased estimators, which serves as an efficient performance benchmark for researchers to identify optimal performance [47], [50]. Generally, authors [18], [20], [51] have derived the CRLB for location estimates and specific model parameters, but they have not addressed scenarios where all model parameters are jointly considered. In this section, we provide the CRLB for the Root Mean Square Error (RMSE) of cooperative RSS-based localization. We encompass scenarios involving unknown transmit power, unknown PLE, and anchor location uncertainty. The fisher information matrix (FIM) of $\boldsymbol{\theta}$ is given in (33), where θ_j denotes the j^{th} element of $\boldsymbol{\theta}$, and $M_1 = 3N_t + 2N_a + 1$. The first and second moments of the RSS and anchor location measurements are given by

$$\mathbb{E}[P_{ij}] = P_j - 10\beta \log_{10} d_{ij}, \quad \text{Var}(P_{ij}) = \sigma_{ij}^2, \quad (34a)$$

$$\mathbb{E}[\mathbf{s}_i] = \check{\mathbf{s}}_i, \quad \text{Var}(\mathbf{s}) = \delta_i^2, \quad (34b)$$

Thus, substituting (2) and (34) into (33) yields

$$\mathbf{F}(\boldsymbol{\theta}) = \mathbf{C}^T \mathbf{Q} \mathbf{C} + \sum_{i \in \mathcal{A}} \delta_i^{-2} \mathbf{R}_i^T \mathbf{R}_i, \quad (35)$$

where

$$\mathbf{C} = \begin{bmatrix} \vdots & \vdots & \vdots & \vdots \\ \mathbf{c}_{ij}^t & \mathbf{c}_{ij}^s & \mathbf{c}_{ij}^p & \mathbf{c}_{ij}^\beta \\ \vdots & \vdots & \vdots & \vdots \end{bmatrix}, \quad j \in \mathcal{T},$$

$$\mathbf{c}_{ij}^t = \left[\mathbf{0}_{1,2(j-1)}, \frac{10\beta (\check{\mathbf{s}}_i - \mathbf{t}_j)^T}{\ln 10 \|\check{\mathbf{s}}_i - \mathbf{t}_j\|^2}, \mathbf{0}_{1,2(N_t-j)} \right], \quad i \in \mathcal{A}_j,$$

$$\mathbf{c}_{ij}^t = \left[\mathbf{0}_{1,2(j-1)}, \mathbf{b}_{ij}^T, \mathbf{0}_{1,2(i-j-1)}, -\mathbf{b}_{ij}^T, \mathbf{0}_{1,2(N_t-i)} \right], \\ i > j, i \in \mathcal{T}_j,$$

$$\mathbf{c}_{ij}^t = \left[\mathbf{0}_{1,2(i-1)}, \mathbf{b}_{ij}^T, \mathbf{0}_{1,2(j-i-1)}, -\mathbf{b}_{ij}^T, \mathbf{0}_{1,2(N_t-j)} \right], \\ i < j, i \in \mathcal{T}_j,$$

$$\mathbf{c}_{ij}^s = \left[\mathbf{0}_{1,2(i-1)}, \frac{10\beta (\mathbf{t}_j - \check{\mathbf{s}}_i)^T}{\ln 10 \|\check{\mathbf{s}}_i - \mathbf{t}_j\|^2}, \mathbf{0}_{1,2(N_a-i)} \right], \quad i \in \mathcal{A}_j,$$

$$\mathbf{c}_{ij}^s = \mathbf{0}_{1,2N_a}, \quad i \in \mathcal{T}_j,$$

$$\mathbf{c}_{ij}^p = [\mathbf{0}_{1,j-1}, 1, \mathbf{0}_{1,N_t-j}], \quad i \in \mathcal{A}_j \cup \mathcal{T}_j,$$

$$\mathbf{c}_{ij}^\beta = -10 \log_{10} \|\mathbf{t}_j - \check{\mathbf{s}}_i\|, \quad i \in \mathcal{A}_j,$$

$$\mathbf{c}_{ij}^\beta = -10 \log_{10} \|\mathbf{t}_j - \mathbf{t}_i\|, \quad i \in \mathcal{T}_j,$$

$$\mathbf{b}_{ij} = \frac{10\beta}{\ln 10} \frac{\mathbf{t}_i - \mathbf{t}_j}{\|\mathbf{t}_i - \mathbf{t}_j\|^2}, \quad i \in \mathcal{T}_j,$$

$$\mathbf{R} = [\mathbf{0}_{2,2N_t+2(i-1)}, \mathbf{I}_2, \mathbf{0}_{2,2(N_a-i)+N_t+1}], \quad i \in \mathcal{A}.$$

Define $M_2 = 2N_t + 2N_a$. Now, the lower bounds of the variance of the estimated parameters are shown as follows:

$$\text{Var}(\hat{\mathbf{t}}_j) \geq \text{tr} \left([\mathbf{F}^{-1}(\boldsymbol{\theta})]_{2j-1:2j, 2j-1:2j} \right), \quad j \in \mathcal{T}, \quad (36a)$$

$$\text{Var}(\hat{P}_j) \geq [\mathbf{F}^{-1}(\boldsymbol{\theta})]_{M_2+j, M_2+j}, \quad j \in \mathcal{T}, \quad (36b)$$

$$\text{Var}(\hat{\beta}) \geq [\mathbf{F}^{-1}(\boldsymbol{\theta})]_{M_1, M_1}. \quad (36c)$$

It is important to obtain the RMSE of the location and transmit power for all target nodes. In numerous practical scenarios,

$$\mathbf{F}(\boldsymbol{\theta}) = \begin{bmatrix} -\mathbb{E} \left[\frac{\partial^2 \ln p(\mathbf{m}; \boldsymbol{\theta})}{\partial \theta_1^2} \right] & \cdots & -\mathbb{E} \left[\frac{\partial^2 \ln p(\mathbf{m}; \boldsymbol{\theta})}{\partial \theta_1 \partial \theta_{M_1}} \right] \\ \vdots & \ddots & \vdots \\ -\mathbb{E} \left[\frac{\partial^2 \ln p(\mathbf{m}; \boldsymbol{\theta})}{\partial \theta_{M_1} \partial \theta_1} \right] & \cdots & -\mathbb{E} \left[\frac{\partial^2 \ln p(\mathbf{m}; \boldsymbol{\theta})}{\partial \theta_{M_1}^2} \right] \end{bmatrix} = \begin{bmatrix} \mathbb{E} \left[\left(\frac{\partial \ln p(\mathbf{m}; \boldsymbol{\theta})}{\partial \theta_1} \right)^2 \right] & \cdots & \mathbb{E} \left[\frac{\partial \ln p(\mathbf{m}; \boldsymbol{\theta})}{\partial \theta_1} \cdot \frac{\partial \ln p(\mathbf{m}; \boldsymbol{\theta})}{\partial \theta_{M_1}} \right] \\ \vdots & \ddots & \vdots \\ \mathbb{E} \left[\frac{\partial \ln p(\mathbf{m}; \boldsymbol{\theta})}{\partial \theta_1} \cdot \frac{\partial \ln p(\mathbf{m}; \boldsymbol{\theta})}{\partial \theta_{M_1}} \right] & \cdots & \mathbb{E} \left[\left(\frac{\partial \ln p(\mathbf{m}; \boldsymbol{\theta})}{\partial \theta_{M_1}} \right)^2 \right] \end{bmatrix} \quad (33)$$

understanding the system's overall performance holds greater significance than concentrating solely on individual nodes. Let the RMSE of estimated parameters be

$$\text{RMSE}(\hat{\mathbf{t}}) = \sqrt{\frac{1}{N_t} \sum_{j \in \mathcal{T}} \|\hat{\mathbf{t}}_j - \mathbf{t}_j\|^2}, \quad (37a)$$

$$\text{RMSE}(\hat{\mathbf{p}}) = \sqrt{\frac{1}{N_t} \sum_{j \in \mathcal{T}} \|\hat{P}_j - P_j\|^2}, \quad (37b)$$

$$\text{RMSE}(\hat{\beta}) = \sqrt{\|\hat{\beta} - \beta\|^2}. \quad (37c)$$

Using (36), we can express the CRLB of the estimated parameters as

$$\text{RMSE}(\hat{\mathbf{t}}) \geq \sqrt{\frac{1}{N_t} \text{tr} \left([\mathbf{F}^{-1}(\boldsymbol{\theta})]_{1:2N_t, 1:2N_t} \right)} \triangleq \text{CRLB}_t, \quad (38a)$$

$$\begin{aligned} \text{RMSE}(\hat{\mathbf{p}}) &\geq \sqrt{\frac{1}{N_t} \text{tr} \left([\mathbf{F}^{-1}(\boldsymbol{\theta})]_{M_2+1: M_2+N_t, M_2+1: M_2+N_t} \right)} \\ &\triangleq \text{CRLB}_p, \end{aligned} \quad (38b)$$

$$\text{RMSE}(\hat{\beta}) \geq \sqrt{[\mathbf{F}^{-1}(\boldsymbol{\theta})]_{M_1, M_1}} \triangleq \text{CRLB}_\beta. \quad (38c)$$

The CRLB for Section III-A, Section III-B, and Section III-C can be similarly calculated by considering $\boldsymbol{\theta} = [\mathbf{t}^T, \mathbf{s}^T]^T$, $\boldsymbol{\theta} = [\mathbf{t}^T, \mathbf{s}^T, \beta]^T$, and $\boldsymbol{\theta} = [\mathbf{t}^T, \mathbf{s}^T, \mathbf{p}^T]^T$, respectively.

V. PERFORMANCE ANALYSIS

In this section, the performance of CTUP is compared with current techniques (refer Table I) with respect to accuracy in estimating location, transmit power, and PLE, alongside computational complexity. The estimation accuracy is verified using both numerical simulations and real-field experimentation. The convergence criterion for iterative techniques (RWLS-AE, RLBM, and IRGDL) is $|\mathbf{J}^k - \mathbf{J}^{k-1}| \leq 10^{-3}$, with \mathbf{J}^k denoting the values of the corresponding objective functions. IRGDL undergoes random initialization, and CTUP-X, along with other SDP-based methods, is implemented using the CVX toolbox, leveraging SeDuMi with the best precision. We choose the normalized root mean squared error (NRMSE) as a performance benchmark

$$\text{NRMSE}_t = \sqrt{\frac{1}{N_t M_c} \sum_{k=1}^{M_c} \sum_{j \in \mathcal{T}} \|\hat{\mathbf{t}}_j^k - \mathbf{t}_j\|^2},$$

$$\text{NRMSE}_p = \sqrt{\frac{1}{N_t M_c} \sum_{k=1}^{M_c} \sum_{j \in \mathcal{T}} \|\hat{P}_j^k - P_j\|^2},$$

$$\text{NRMSE}_\beta = \sqrt{\frac{1}{M_c} \sum_{k=1}^{M_c} \|\hat{\beta}^k - \beta\|^2},$$

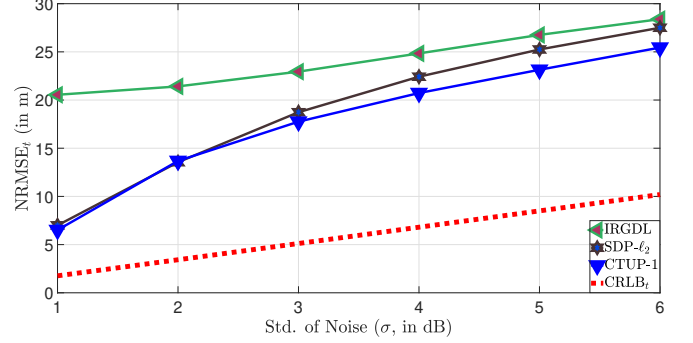


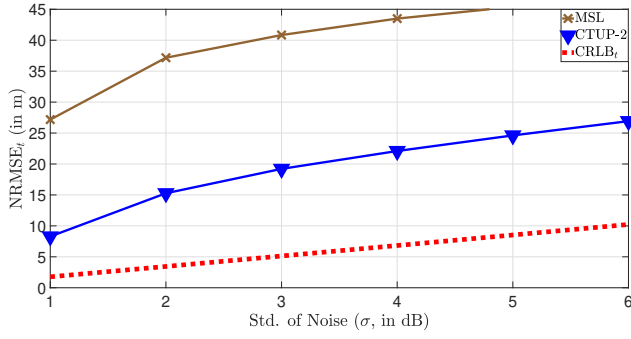
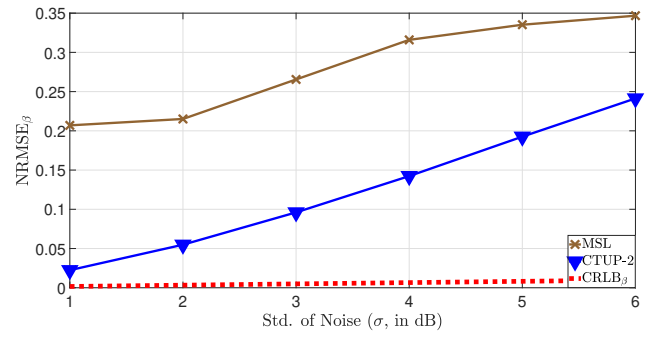
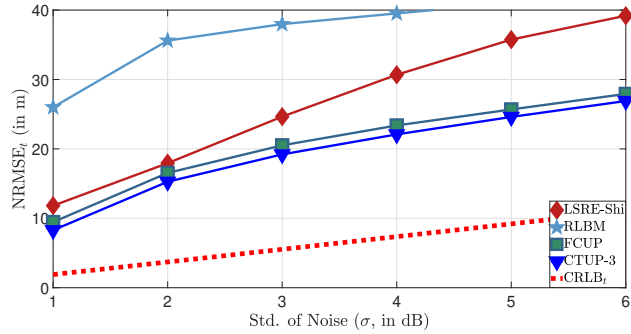
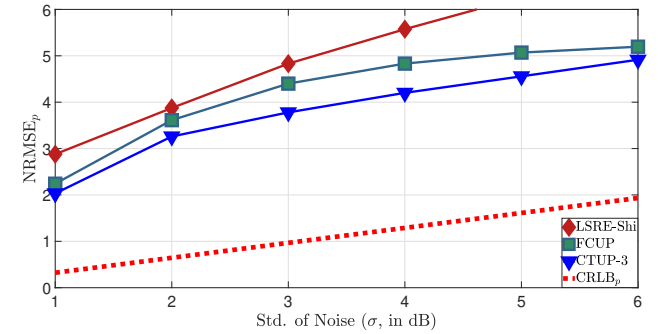
Fig. 1. Performance of the localization techniques for scenarios where transmit power and PLE are known ($\delta = 3$ m).

where M_c is the number of Monte-Carlo simulations. All the simulation results presented in the paper are obtained using 3000 Monte-Carlo simulations.

A. Numerical simulations

The performance of localization techniques is evaluated for four scenarios discussed in Section III. We employ two networks, denoted as NW-1 and NW-2, to study the impact of noise and anchor location uncertainty, respectively. NW-1 consists of 5 anchor nodes and 10 target nodes, and NW-2 consists of 20 anchor nodes and 10 target nodes. In both NW-1 and NW-2, the target nodes and anchor nodes are randomly deployed over an area of 100×100 m², with fixed locations throughout the simulations. NW-1 and NW-2 are assumed to be fully connected in the simulations, enabling all anchor nodes and target nodes to communicate interchangeably. The transmit power of target nodes is randomly selected from a uniform distribution between [-10 10] dBm, and the path loss exponent (β) in (1a) is set to 3. Without loss of generality, we assume that $\sigma_{ij} = \sigma$ and $\delta_i = \delta$ [14], [52]. All the results presented in Section V-A1, Section V-A2, Section V-A3, and Section V-A4 are obtained using NW-1 and the simulation results shown in Section V-A5 are based on NW-2.

1) *Scenario I*: We compare the performance of CTUP-1 with IRGDL [21] and SDP- ℓ_2 [22] when the transmit power of the nodes and PLE are known. Fig. 1 demonstrates that CTUP-1 outperforms SDP- ℓ_2 and IRGDL for all values of σ . This occurs because SDP- ℓ_2 and IRGDL are affected by both σ and δ , while CTUP-1 mitigates the influence of anchor location uncertainty. For low noise scenarios, the performance of SDP- ℓ_2 and CTUP-1 are similar; however, its effectiveness diminishes notably in scenarios where $\sigma > 3$ dB. The variations in σ have less impact on the NRMSE of IRGDL,

(a) NRMSE of location estimate as a function of σ .(b) NRMSE of PLE estimate as a function of σ .Fig. 2. Performance of the localization techniques for scenarios where PLE is unknown ($\delta = 3$ m).(a) NRMSE of location estimate as a function of σ .(b) NRMSE of transmit power estimate as a function of σ .Fig. 3. Performance of the localization techniques for scenarios where transmit power is unknown ($\delta = 3$ m).TABLE III
COMPUTATIONAL COMPLEXITY OF EXISTING TECHNIQUES.

Algo.	Manner	Computational complexity	CPU runtime (in s)		Year
			T_1	T_2	
LSRE-Shi	Non-cooperative	$\mathcal{O}(N_t \sqrt{N_a} + 2(N_a + 4)^3)$	12.41	13.17	2020
RWLS-AE	Non-cooperative	$\mathcal{O}(N_t N_a^{6.5} \sum_{j \in \mathcal{T}} i_j^{\text{itr}})$	92.03	153.06	2021
SDP-Zou	Non-cooperative	$\mathcal{O}((N_t + N_a) N_t N_a^{6.5})$	18.41	94.71	2021
RLBM	Non-cooperative	$\mathcal{O}(N_t (N_a^4 + 7N_a^2) \sum_{j \in \mathcal{T}} i_j^{\text{itr}})$	11.02	11.63	2021
MSL	Non-cooperative	$\mathcal{O}(N_t)$	0.001	0.002	2022
IRGDL	Cooperative	$\mathcal{O}(\mathcal{H} k^{\text{itr}})$	0.07	0.07	2022
SDP- ℓ_2	Cooperative	$\mathcal{O}(\sqrt{2N_t(N_t + N_a)} (2N_t)^4 (N_t + N_a)^4)$	9.06	17.75	2022
FCUP	Cooperative	$\mathcal{O}(N_t^{0.5} (\mathcal{H} ^2 N_a (N_t + 2)^2 + \mathcal{H} (N_t + 2)^3))$	2.29	2.68	2023
CTUP-1	Cooperative	$\mathcal{O}(N_t^{0.5} (\mathcal{H} ^4 + \mathcal{H} ^2 (N_t + 2)^2 + \mathcal{H} (N_t + 2)^3 + \mathcal{H} ^3))$	2.74	3.88	2023
CTUP-2			2.81	4.12	
CTUP-3			2.79	4.08	
CTUP-4			2.87	4.21	

yet it exhibits high localization error. This is due to the loss of information caused by inverting the ML objective function.

2) *Scenario II*: In the scenario of unknown β , we compare the performance of CTUP-2 with MSL [20] in terms of the location estimate and PLE estimate. The performance of localization techniques is studied when PLE is unknown. The NRMSE of the location estimate as a function of σ is presented in Fig. 2(a). CTUP-2 demonstrates superior performance compared with MSL for considered scenarios. As the σ increases, the performance gap between MSL and CTUP-2 widens, primarily due to the limitations of LLS in managing high-noise scenarios. In Fig. 2(b), it can be observed that CTUP-2

outperforms MSL in the estimate of PLE.

3) *Scenario III*: In the case of unknown transmit power, we evaluate the performance of CTUP-3, LSRE-Shi [16], RLBM [19], and FCUP [23] in estimating the location and transmit power of target nodes. The performance of the localization techniques is shown in Fig. 3(a). CTUP-3 and FCUP exhibit comparable performances, surpassing other techniques. However, CTUP-3 showcases superior performance over FCUP due to FCUP's lack of consideration for anchor location uncertainty. CTUP-3 outperforms LSRE-Shi and FCUP in estimating the transmit power, as shown in Fig. 3(b). RLBM and LSRE-Shi demonstrate inferior per-

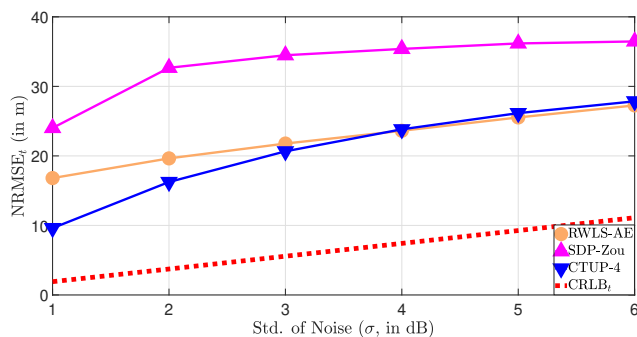
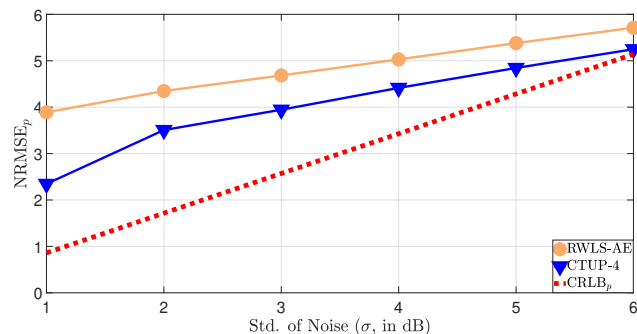
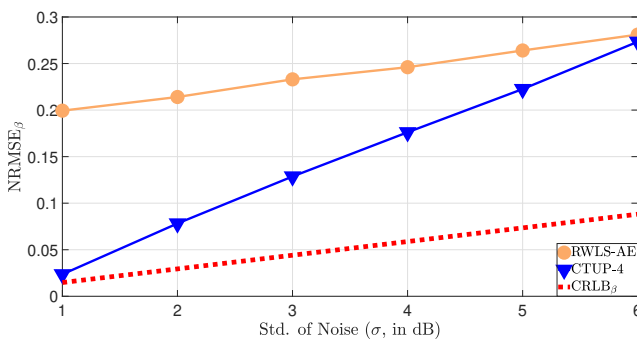
(a) NRMSE of location estimate as a function of σ .(b) NRMSE of transmit power estimate as a function of σ .(c) NRMSE of PLE estimate as a function of σ .

Fig. 4. Performance of the localization techniques for scenarios where transmit power and PLE are unknown ($\delta = 3$ m).

formance since they do not incorporate RSS readings of the target-target links.

4) *Scenario IV*: In the fourth scenario where transmit power and PLE are unknown, we evaluate CTUP-4's performance in comparison to RWLS-AE [17] and SDP-Zou [18]. In Fig. 4(a), we present the localization accuracy of the techniques as a function of σ . CTUP-4 outperforms RWLS-AE and SDP-Zou at low noise levels. Although RWLS-AE performs slightly better than CTUP-4 at high noise levels, it has the highest computational complexity among the compared techniques (refer Table III). The accuracy of the transmit power estimate as a function of σ is illustrated in Fig. 4(b), where CTUP-4 outperforms RWLS-AE across all values of σ . In Fig. 4(c), we present NRMSE $_{\beta}$ as a function of the noise standard deviation. CTUP-4 achieves the best performance, especially at low noise levels. RWLS-AE demonstrates comparable performance to CTUP-4 when $\sigma > 6$ dB. However, The

noise standard deviation is typically less than 4 dB in practical scenarios (refer Table IV), thereby indicating the superior performance of CTUP-4 in the realistic implementation.

5) *Effect of the anchor location uncertainty*: In this section, we study the performance of localization techniques as a function of δ (refer Fig. 5(a)). Across all δ values, CTUP-4 outperforms other existing techniques. When δ is small, LSRE-Shi has a performance similar to CTUP-4; however, in scenarios where $\delta > 5$ dBm, its effectiveness decreases significantly. In Fig. 5(b), CTUP-4 shows superior performance in estimating the transmit power of target nodes. Although RWLS-AE and CTUP-4 are less influenced by anchor location uncertainty, CTUP-4's transmit power estimate is closest to CRLB $_p$, highlighting its increasing superiority with greater uncertainty in anchor locations. In conclusion, numerical simulations have verified the effectiveness of proposed techniques in considered scenarios. CTUP shows superior performance in estimating location, transmit power, and PLE compared to existing techniques.

6) *Non-cooperative localization*: In this section, we evaluate the performance of localization techniques in non-cooperative scenarios. We utilize two networks, denoted as NW-3 and NW-4, to examine the effects of noise standard deviation and anchor location uncertainty, respectively. NW-3 and NW-1 share identical configurations except for NW-3 containing only one randomly deployed target node. Similarly, NW-4 and NW-2 have identical configurations, with NW-4 featuring only one randomly deployed target node. Simulation results presented in Fig. 6(a) and Fig. 6(b) are obtained from NW-3 and NW-4, respectively. We study the performance of localization techniques as a function σ in Fig. 6(a). CTUP-4 demonstrates superior performance across most scenarios. Despite RWLS-AE marginally outperforming CTUP-4 for $\sigma > 5$ dB, It has the highest complexity (refer to Table III). The performance order of localization techniques is similar to that observed in cooperative scenarios. Fig. 6(b) presents the localization performance as a function of δ . Similar to the scenario depicted in Fig. 5(a), LSRE-Shi and CTUP-4 exhibit comparable performance when $\delta < 5$ m. However, CTUP-4 significantly surpasses LSRE-Shi for $\delta > 5$ m. While RWLS-AE outperforms CTUP-4 for $\delta > 15$ m, it has extremely high complexity. Overall, CTUP-4 exhibits superior performance compared to existing techniques in non-cooperative scenarios.

B. Complexity comparison

The computational complexity of localization techniques is provided in Table III. We consider only the dominant elements to compute the computational complexity to ensure consistency with compared localization techniques [16]–[23]. In Table III, we compute the CPU runtime of all techniques in MATLAB R2021a using an Intel(R) Xeon(R) W-2245 CPU @ 3.90GHz processor with 64GB RAM. RLBM and RWLS-AE are non-cooperative iterative techniques, whereas IRGDL is a cooperative technique utilizing gradient descent. Therefore, in Table III, we employ two distinct notations to represent the number of iterations required for convergence. For RLBM and RWLS-AE, i_j^{tr} denotes the iteration count necessary

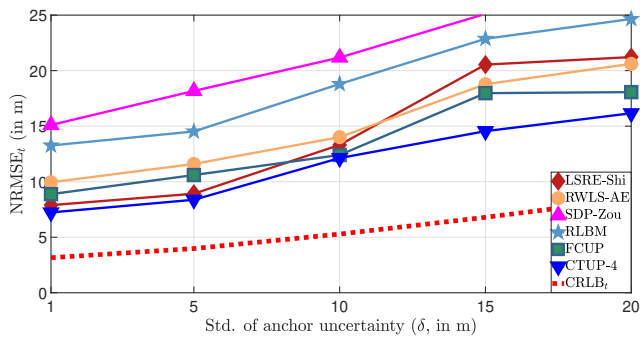
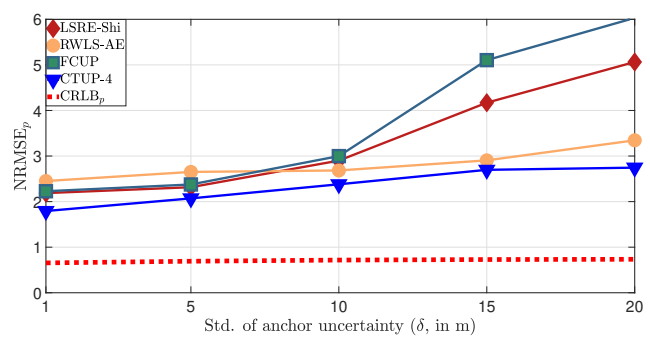
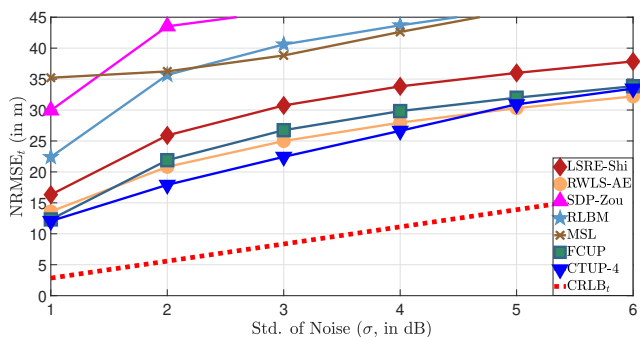
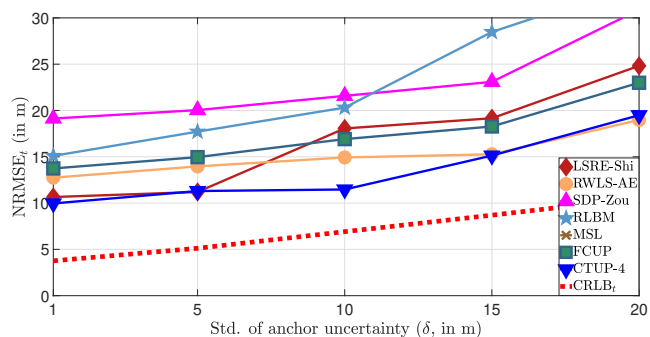
(a) NRMSE of location estimate as a function of δ .(b) NRMSE of transmit power estimate as a function of δ .Fig. 5. Performance of the localization techniques with respect to the anchor location uncertainty ($\sigma = 3$ dB).(a) NRMSE of location estimate as a function of σ .(b) NRMSE of location estimate as a function of δ .

Fig. 6. Performance of the localization techniques in non-cooperative scenarios.



Fig. 7. Photographs of the localization experimental site and setups.

for the j^{th} target node to converge. In IRGDL, k^{itr} denotes

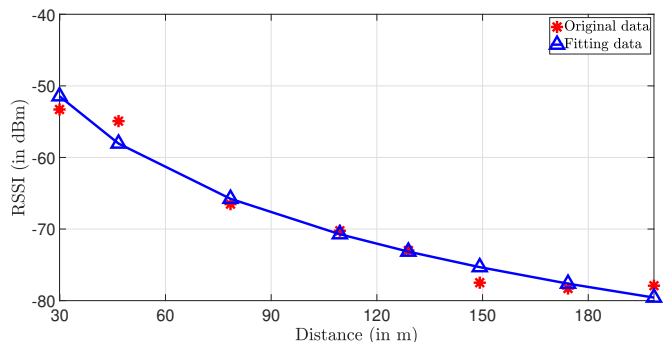
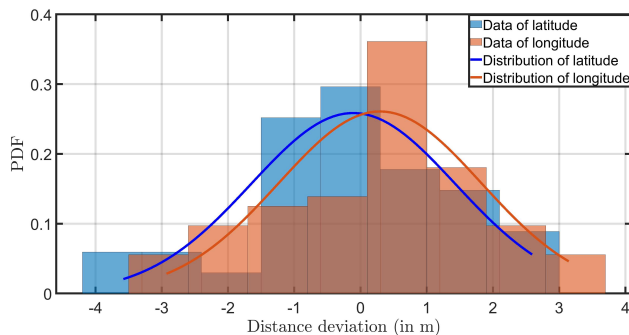
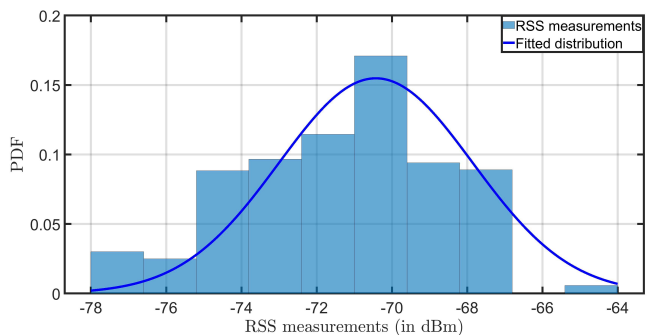


Fig. 8. Fit the log-normal model to estimate the transmit power and PLE.

the number of steps taken for gradient descent to achieve convergence. T_1 and T_2 represent the CPU running time of the localization techniques for NW-1 and NW-2, respectively. It can be observed in Table III that MSL has the least complexity, however, it exhibits significantly poor localization accuracy (refer Fig. 2). Non-cooperative techniques usually have high computational complexity since they are required to solve an SDP problem for each target node. IRGDL benefits from the simplicity of gradient descent, with its computational complexity increasing linearly in accordance with the network's size. Nevertheless, it demonstrates poor performance, as can be observed in Fig. 1. The computational complexity of SDP- ℓ_2 scales proportionally to $N_t^{8.5}$, whereas CTUPs exhibit a computational complexity of $\sim N_t^{6.5}$, making them suitable for dense networks. However, CTUP-2 and CTUP-4 require



(a) The distribution of gathered latitude and longitude readings.



(b) The distribution of RSS measurements.

Fig. 9. The distribution of gathered experimental data: a) anchor location readings, and b) RSS measurements.

additional time as they leverage links between anchor nodes prior to solving the mixed SDP-SOCP problem. CTUP-3 takes slightly longer than CTUP-1 due to the additional step of extracting the estimate of the transmit power. In comparison to FCUP, the CTUPs have marginally higher CPU runtime. However, this trade-off allows them to address the impact of anchor location uncertainty effectively and also consider scenarios where PLE is unknown (refer Section III-D), leading to enhanced performance (refer Fig. 3 and Fig. 5).

C. Experimental results

Real-world network experiments are significant for the implementation and analysis of cooperative localization techniques [53]. We carried out extensive real-field experiments to further validate the effectiveness of localization techniques. We use the RAK 4631 [54] to establish a Bluetooth low energy (BLE) mesh network employing an omnidirectional BLE antenna with a gain of 2 dBi [55]. The RSS measurements among the nodes are uploaded to the data center using a LoRa transceiver. The precise location of the nodes, accurate to the centimeter level, is obtained using real-time kinematic (RTK) GPS, serving as the ground truth. We also collected the location of the anchor nodes using standard GPS, providing meter-level accuracy. The imprecision associated with these readings is referred to as “anchor location uncertainty”. Each node is equipped with a solar panel and a lithium battery to ensure long-term operation. The nodes are mounted on aluminium poles, each standing at a height of 1 meter. Across a vast outdoor expanse measuring $640 \times 180 m^2$, we deploy a total of 50 nodes. The photographs of the experiment site and the node are shown in Fig. 7. Although the transmit power and PLE are not required for CTUP-4, these parameters are essential to implement other localization techniques. To obtain the transmit power of the nodes and PLE, we placed 9 nodes in a straight-line configuration. One node is configured as the BLE transmitter, and the remaining nodes are the BLE listener. Fig. 8 shows the variation of RSS as a function of distance. We estimated the transmit power of the node and PLE by applying the log-normal model (refer (1a)) to the dataset. The network details are shown in Table IV.

We gathered approximately 100 location readings of a node using a standard GPS, while the precise location was

TABLE IV
PARAMETERS OF THE EXPERIMENTAL SITE.

Area (in m^2)	$640 \times 180 m^2$
Number of nodes	50
Received RSS readings per link	~ 500
The nodes' height	1 m
Transmit power (in dBm)	-3.59
PLE	3.27
Average noise standard deviation (in dB)	2.47
Average anchor location uncertainty (in m)	1.53

determined using RTK GPS. Fig. 9(a) showcases the deviations in latitude and longitude of the GPS data compared to the precise location. We employed the MATLAB routine `histogram(data, N_b , 'Normalization', 'pdf')` to normalize the counts within each bin, where `data` represents the readings of interest, and N_b stands for the number of bins. We select N_b employing Sturges' rule [56], [57]: $N_b = \lceil 1 + \log_2(N_d) \rceil$, where N_d denotes the total sample size, and $\lceil \cdot \rceil$ represents the ceiling function. Our dataset comprises of 100 location readings from a single GPS node, hence, N_b is set to be 8 bins. In Fig. 9(a), the mean deviation for latitude is -0.11 m, and for longitude, it is 0.29 m. Moreover, the standard deviation for longitude and latitude measurements is ~ 1.53 m. Therefore, Fig. 9(a) demonstrates that the anchor location uncertainties for both latitude and longitude follow a common zero-mean Gaussian distribution, affirming the efficacy of our considered model (1b). Fig. 9(b) depicts the distribution of 500 RSS readings from a BLE communication link. The mean value and standard deviation are -70.43 dBm and 2.57 dB, respectively. Given the distance between the two nodes as 86.23 m, utilizing (1a) and parameters from Table IV, the mean value and standard deviation of RSS measurements in this link are computed as -66.88 dBm and 2.47 dB, respectively. These values align with Fig. 9(b), affirming the effectiveness of our approach in obtaining experimental parameters. In addition, Fig. 9(b) demonstrates that RSS measurements follow a Gaussian distribution. Moreover, as RSS measurements and anchor locations are mutually independent, the efficacy of (2) can be confirmed.

The performance of localization techniques is evaluated using the experimental data, with each node receiving a

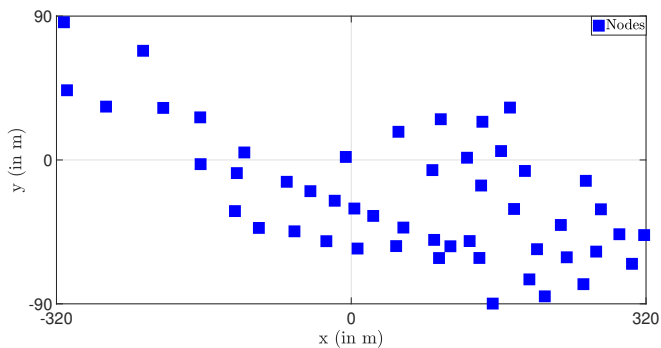
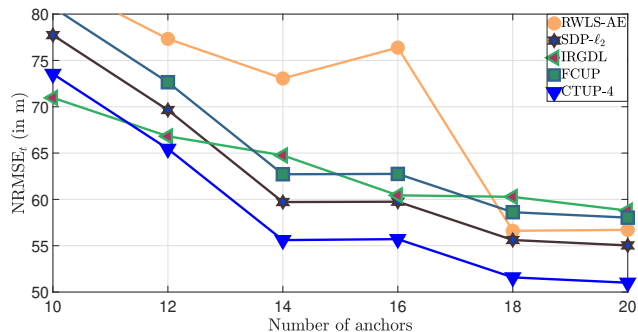
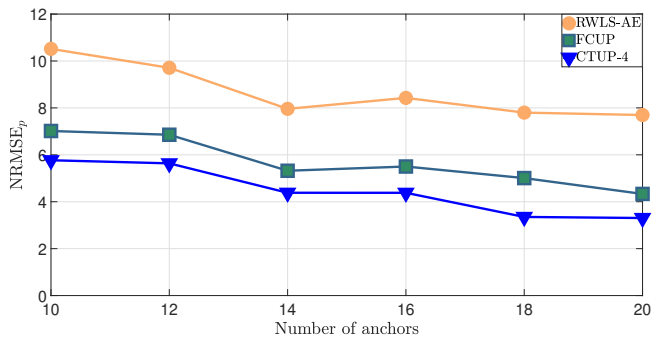


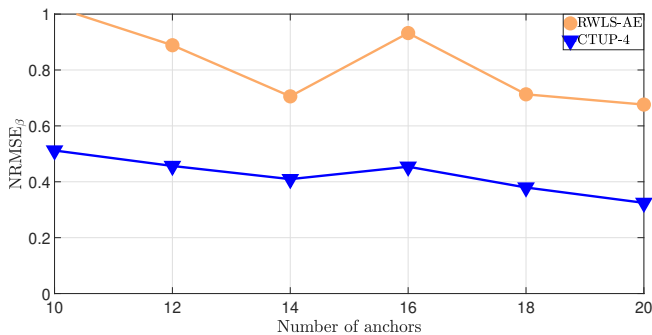
Fig. 10. The network utilized in the experiment, comprising 50 nodes.



(a) NRMSE of location estimate as a function of the number of anchor nodes.



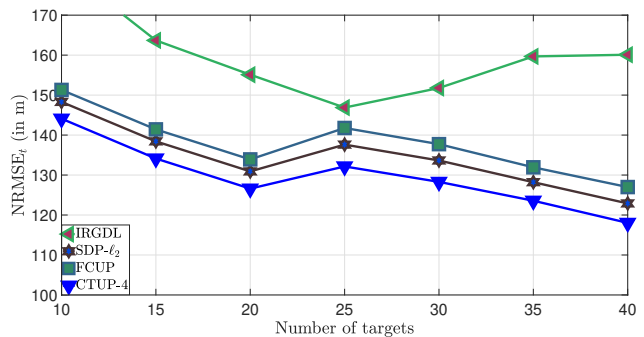
(b) NRMSE of transmit power estimate as a function of the number of anchor nodes.



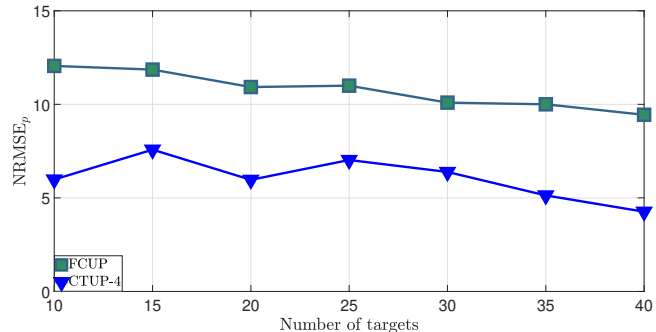
(c) NRMSE of PLE estimate as a function of the number of anchor nodes.

Fig. 11. Localization performance as a function of anchor node numbers utilizing experimental data.

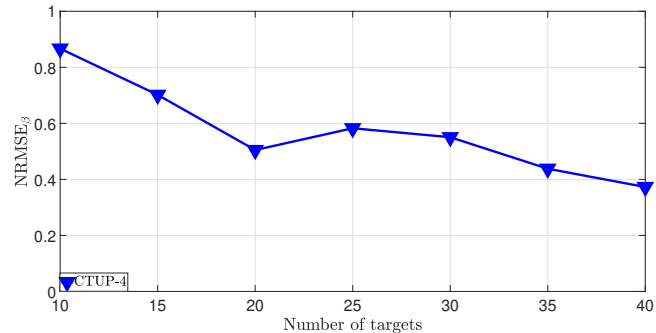
minimum of 500 readings. Fig. 10 displays the topology of the network consisting of 50 nodes.



(a) NRMSE of location estimate as a function of the number of target nodes.



(b) NRMSE of transmit power estimate as a function of the number of target nodes.



(c) NRMSE of PLE estimate as a function of the number of target nodes.

Fig. 12. Localization performance as a function of target node numbers using experimental data.

1) *Effect of the number of anchor nodes:* In this study, we randomly selected 10 target nodes to explore the impact of varying the number of anchor nodes on the location algorithms. In Fig. 11(a), we present the performance of the localization technique as a function of the number of anchor nodes (N_a). LSRE-Shi, SDP-Zou, RLBM, and MSL are excluded from Fig. 11(a) due to their poor performance. Fig. 11(a) demonstrates that the increase in the number of anchor nodes tends to decrease the NRMSE of the location estimate. Non-cooperative techniques fail to achieve high accuracy since they cannot leverage the target-target links. CTUP-4 outperforms FCUP and SDP- l_2 by effectively mitigating the impact of anchor location uncertainty. IRGDL exhibits marginally superior performance compared to CTUP-4 at $N_a = 10$; however, as N_a increases, IRGDL's performance deteriorates. This occurs since the error induced by the invex

relaxation method escalates alongside the growing number of available links, resulting in a situation where IRGDL gains fewer benefits from the increased number of anchor nodes compared to SDP-based techniques.

We utilize the transmit power and PLE presented in Table IV as ground truths to evaluate the accuracy of localization techniques in estimating transmit power and PLE. The accuracy of the transmit power estimate with respect to the of number anchor node is depicted in Fig. 11(b). From Fig. 11(b) it can be observed that CTUP-4 outperforms RWLS-AE and FCUP across all considered scenarios. In Fig. 11(c), we compare the NRMSE_β of CTUP-4 with that of RWLS-AE as a function of the number of anchor nodes, with CTUP-4 demonstrating superior performance.

2) *Effect of the number of target nodes*: Fig. 12(a) displays the performance of the location techniques as the number of target nodes is increased. Non-cooperative techniques are not included as they cannot leverage the target-target links. A tendency of performance enhancement is observed with the rising number of target nodes due to additional RSS measurements obtained from new links. CTUP-4 shows the best performance in comparison to other techniques. In Fig. 12(b), CTUP-4 demonstrates superior performance compared to existing localization techniques. While CTUP-4 uniquely possesses the capability to estimate PLE among cooperative techniques (refer to Table I), we present its performance in Fig. 12(c). It's noteworthy that the performance enhancement resulting from an increased number of target nodes is less significant compared to the improvements obtained from expanding the number of anchor nodes. This disparity arises because, with an increase in target nodes, more decision variables (such as the location and transmit power of new nodes) are introduced to the optimization problem.

VI. CONCLUSION

In this paper, we have addressed cooperative RSS-based localization in scenarios involving unknown transmit power, PLE, and anchor location uncertainty. We have proposed localization techniques (CTUPs) using mixed SDP-SOCP to jointly estimate target nodes' location, transmit power, and PLE. The reformulation of the ML estimator employs Taylor expansion, SDR, and the epigraph method, leveraging the accuracy of SDP and the computational efficiency of SOCP. We have carried out comprehensive simulations to demonstrate CTUPs' superior performance in terms of estimation accuracy and computational complexity compared to existing localization techniques. We have conducted extensive real-field experiments to curate an indigenous dataset encompassing RSS measurements among 50 nodes (with anchor location uncertainty) and further validate the effectiveness of CTUPs. Our future work will focus on developing localization techniques in the presence of malicious nodes, aiming to enhance robustness and security in cooperative localization.

REFERENCES

- [1] S. Chen, B. Liu, C. Feng, C. Vallespi-Gonzalez, and C. Wellington, "3D point cloud processing and learning for autonomous driving: Impacting map creation, localization, and perception," *IEEE Signal Process. Mag.*, vol. 38, no. 1, pp. 68–86, Jan. 2021.
- [2] Y. Zou, H. Liu, and Q. Wan, "Joint synchronization and localization in wireless sensor networks using semidefinite programming," *IEEE Internet Things J.*, vol. 5, no. 1, pp. 199–205, Feb. 2018.
- [3] X. Ma, B. Hao, H. Zhang, and P. Wan, "Semidefinite relaxation for source localization by TOA in unsynchronized networks," *IEEE Signal Process. Lett.*, vol. 29, pp. 622–626, Feb. 2022.
- [4] A. Pandey, P. Tiwary, S. Kumar, and S. K. Das, "Fadeloc: Smart device localization for generalized κ - μ faded IoT environment," *IEEE Trans. Signal Process.*, vol. 70, pp. 3206–3220, Jun. 2022.
- [5] M. Z. Win, F. Meyer, Z. Liu, W. Dai, S. Bartoletti, and A. Conti, "Efficient Multisensor Localization for the Internet of Things: Exploring a New Class of Scalable Localization Algorithms," *IEEE Signal Process. Mag.*, vol. 35, no. 5, pp. 153–167, Sep. 2018.
- [6] T. Stoyanova, F. Kerasiotis, C. Antonopoulos, and G. Papadopoulos, "RSS-based localization for wireless sensor networks in practice," in *2014 9th International Symposium on Communication Systems, Networks & Digital Sign (CSNDSP)*, Jul. 2014, pp. 134–139.
- [7] M. Z. Win, A. Conti, S. Mazuelas, Y. Shen, W. M. Gifford, D. Dardari, and M. Chiani, "Network localization and navigation via cooperation," *IEEE Commun. Mag.*, vol. 49, no. 5, pp. 56–62, May. 2011.
- [8] Z. Liu, W. Dai, and M. Z. Win, "Mercury: An Infrastructure-Free System for Network Localization and Navigation," *IEEE Trans. Mob. Comput.*, vol. 17, no. 5, pp. 1119–1133, May. 2018.
- [9] Y. Sun, K. C. Ho, and Q. Wan, "Eigenspace solution for AOA localization in modified polar representation," *IEEE Trans. Signal Process.*, vol. 68, pp. 2256–2271, Mar. 2020.
- [10] X. Ma, B. Hao, H. Zhang, and P. Wan, "Semidefinite relaxation for source localization by TOA in unsynchronized networks," *IEEE Signal Process. Lett.*, vol. 29, pp. 622–626, Feb. 2022.
- [11] K. C. Ho and T.-K. Le, "Integrating AOA with TDOA for joint source and sensor localization," *IEEE Trans. Signal Process.*, vol. 71, pp. 2087–2102, May. 2023.
- [12] B. Mukhopadhyay, S. Srirangarajan, and S. Kar, "RSS-based cooperative localization and edge node detection," *IEEE Trans. Veh. Technol.*, vol. 71, no. 5, pp. 5387–5403, Feb. 2022.
- [13] A. Coluccia and A. Fascista, "On the hybrid TOA/RSS range estimation in wireless sensor networks," *IEEE Trans. Wirel. Commun.*, vol. 17, no. 1, pp. 361–371, Jan. 2018.
- [14] R. M. Vaghefi, M. R. Gholami, R. M. Buehrer, and E. G. Strom, "Cooperative received signal strength-based sensor localization with unknown transmit powers," *IEEE Trans. Signal Process.*, vol. 61, no. 6, pp. 1389–1403, Dec. 2013.
- [15] S. Yang, G. Wang, Y. Hu, and H. Chen, "Robust differential received signal strength based localization with model parameter errors," *IEEE Signal Process. Lett.*, vol. 25, no. 11, pp. 1740–1744, Nov. 2018.
- [16] J. Shi, G. Wang, and L. Jin, "Least squared relative error estimator for RSS based localization with unknown transmit power," *IEEE Signal Process. Lett.*, vol. 27, pp. 1165–1169, Jun. 2020.
- [17] Y. Sun, S. Yang, G. Wang, and H. Chen, "Robust RSS-based source localization with unknown model parameters in mixed LOS/NLOS environments," *IEEE Trans. Veh. Technol.*, vol. 70, no. 4, pp. 3926–3931, Mar. 2021.
- [18] Y. Zou and H. Liu, "RSS-based target localization with unknown model parameters and sensor position errors," *IEEE Trans. Veh. Technol.*, vol. 70, no. 7, pp. 6969–6982, Jun. 2021.
- [19] H. Lohrasbipeydeh and T. A. Gulliver, "RSSD-based MSE-SDP source localization with unknown position estimation bias," *IEEE Trans. Commun.*, vol. 69, no. 12, pp. 8416–8428, Sep. 2021.
- [20] X. Mei, Y. Chen, X. Xu, and H. Wu, "RSS localization using multistep linearization in the presence of unknown path loss exponent," *IEEE Sens. Lett.*, vol. 6, no. 8, pp. 1–4, Aug. 2022.
- [21] B. Mukhopadhyay, S. Srirangarajan, and S. Kar, "Invox relaxation based cooperative localization using RSS measurements," *IEEE Trans. Commun.*, vol. 70, no. 8, pp. 5482–5497, Jun. 2022.
- [22] Q. Wang, Z. Duan, and F. Li, "Semidefinite programming for wireless cooperative localization using biased RSS measurements," *IEEE Commun. Lett.*, vol. 26, no. 6, pp. 1278–1282, Apr. 2022.
- [23] Y. Li, B. Mukhopadhyay, and M.-S. Alouini, "RSS-based cooperative localization and transmit power(s) estimation using mixed SDP-SOCP," *IEEE Trans. Veh. Technol.*, pp. 1–6, Jul. 2023.
- [24] H. C. So and L. Lin, "Linear least squares approach for accurate received signal strength based source localization," *IEEE Trans. Signal Process.*, vol. 59, no. 8, pp. 4035–4040, Aug. 2011.
- [25] G. Wang and K. Yang, "A new approach to sensor node localization using RSS measurements in wireless sensor networks," *IEEE Trans. Wireless Commun.*, vol. 10, no. 5, pp. 1389–1395, Mar. 2011.

- [26] C. Soares, J. Xavier, and J. Gomes, "Simple and fast convex relaxation method for cooperative localization in sensor networks using range measurements," *IEEE Trans. Signal Process.*, vol. 63, no. 17, pp. 4532–4543, Jul. 2015.
- [27] N. Piovesan and T. Erseghe, "Cooperative localization in WSNs: A hybrid convex/nonconvex solution," *IEEE Trans. Signal Inf.*, vol. 4, no. 1, pp. 162–172, Dec. 2018.
- [28] S. Chang, Y. Li, H. Wang, W. Hu, and Y. Wu, "RSS-based cooperative localization in wireless sensor networks via second-order cone relaxation," *IEEE Access*, vol. 6, pp. 54 097–54 105, Sep. 2018.
- [29] K. N. R. S. V. Prasad and V. K. Bhargava, "Rss localization under gaussian distributed path loss exponent model," *IEEE Wireless Communications Letters*, vol. 10, no. 1, pp. 111–115, 2021.
- [30] Z. Wang, H. Zhang, T. Lu, and T. A. Gulliver, "Cooperative RSS-based localization in wireless sensor networks using relative error estimation and semidefinite programming," *IEEE Trans. Veh. Technol.*, vol. 68, no. 1, pp. 483–497, Nov. 2019.
- [31] H. Xiong, M. Peng, S. Gong, and Z. Du, "A novel hybrid RSS and TOA positioning algorithm for multi-objective cooperative wireless sensor networks," *IEEE Sens. J.*, vol. 18, no. 22, pp. 9343–9351, Sep. 2018.
- [32] N. Saeed, A. Celik, T. Y. Al-Naffouri, and M.-S. Alouini, "Localization of energy harvesting empowered underwater optical wireless sensor networks," *IEEE Trans. Wireless Commun.*, vol. 18, no. 5, pp. 2652–2663, May. 2019.
- [33] J. Choi, "Sensor-aided learning for Wi-Fi positioning with beacon channel state information," *IEEE Trans. Wireless Commun.*, vol. 21, no. 7, pp. 5251–5264, Jul. 2022.
- [34] A. Nagy, T. Bigler, A. Treytl, R. Stenzl, S. Wilker, T. Sauter, and T. Wien, "RSS-based localization for directional antennas," in *2020 25th IEEE International Conference on Emerging Technologies and Factory Automation (ETFA)*, vol. 1, Sep. 2020, pp. 774–781.
- [35] M. K. Simon and M.-S. Alouini, *Digital Communication over Fading Channels*. New York: Wiley, 2001.
- [36] J. Miranda, R. Abrishambaf, T. Gomes, P. Gonçalves, J. Cabral, A. Tavares, and J. Monteiro, "Path loss exponent analysis in wireless sensor networks: Experimental evaluation," in *2013 11th IEEE International Conference on Industrial Informatics (INDIN)*, Jul. 2013, pp. 54–58.
- [37] S.-H. Kim, S.-W. Moon, D.-G. Kim, M. Ko, and Y.-H. Choi, "A neural network-based path loss model for bluetooth transceivers," in *2022 International Conference on Information Networking (ICOIN)*, Jan. 2022, pp. 446–449.
- [38] S. Sun, T. S. Rappaport, T. A. Thomas, A. Ghosh, H. C. Nguyen, I. Z. Kovács, I. Rodriguez, O. Koymen, and A. Partyka, "Investigation of prediction accuracy, sensitivity, and parameter stability of large-scale propagation path loss models for 5G wireless communications," *IEEE Trans. Veh. Technol.*, vol. 65, no. 5, pp. 2843–2860, May. 2016.
- [39] M. R. Gholami, R. M. Vaghefi, and E. G. Ström, "RSS-based sensor localization in the presence of unknown channel parameters," *IEEE Trans. Signal Process.*, vol. 61, no. 15, pp. 3752–3759, Aug. 2013.
- [40] L. Wu, D. He, B. Ai, J. Wang, H. Qi, K. Guan, and Z. Zhong, "Artificial neural network based path loss prediction for wireless communication network," *IEEE Access*, vol. 8, pp. 199 523–199 538, Nov. 2020.
- [41] Y. Xu, J. Zhou, and P. Zhang, "RSS-based source localization when path-loss model parameters are unknown," *IEEE Commun. Lett.*, vol. 18, no. 6, pp. 1055–1058, Jun. 2014.
- [42] A. G. Dempster and E. Cetin, "Interference localization for satellite navigation systems," *Proc. IEEE*, vol. 104, no. 6, pp. 1318–1326, Jun. 2016.
- [43] H. Lohrasbipeydeh, T. A. Gulliver, and H. Amindavar, "Unknown transmit power RSSD based source localization with sensor position uncertainty," *IEEE Trans. Commun.*, vol. 63, no. 5, pp. 1784–1797, May. 2015.
- [44] P. Barsocchi, S. Lenzi, S. Chessa, and G. Giunta, "A novel approach to indoor RSSI localization by automatic calibration of the wireless propagation model," in *VTC Spring 2009 - IEEE 69th Vehicular Technology Conference*, Apr. 2009, pp. 1–5.
- [45] H. Lim, L.-C. Kung, J. C. Hou, and H. Luo, "Zero-configuration, robust indoor localization: Theory and experimentation," in *Proceedings IEEE INFOCOM 2006. 25TH IEEE International Conference on Computer Communications*, Apr. 2006, pp. 1–12.
- [46] A. Coluccia and F. Ricciato, "On ML estimation for automatic RSS-based indoor localization," in *IEEE 5th International Symposium on Wireless Pervasive Computing 2010*, May. 2010, pp. 495–502.
- [47] S. M. Kay, *Fundamentals of Statistical Signal Processing*. Prentice Hall PTR, 1993.
- [48] L. Vandenberghe and S. Boyd, "Semidefinite programming," *SIAM review*, vol. 38, no. 1, pp. 49–95, 1996.
- [49] M. Grant and S. Boyd, "CVX: Matlab software for disciplined convex programming, version 2.1," <http://cvxr.com/cvx>, Mar. 2014.
- [50] N. Patwari, J. Ash, S. Kyperountas, A. Hero, R. Moses, and N. Correal, "Locating the nodes: cooperative localization in wireless sensor networks," *IEEE Signal Process. Mag.*, vol. 22, no. 4, pp. 54–69, Jul. 2005.
- [51] S. Tomic *et al.*, "RSS-based localization in wireless sensor networks using convex relaxation: Noncooperative and cooperative schemes," *IEEE Trans. Veh. Technol.*, vol. 64, no. 5, pp. 2037–2050, Jul. 2015.
- [52] Y. Zou and H. Liu, "Semidefinite programming methods for alleviating clock synchronization bias and sensor position errors in TDOA localization," *IEEE Signal Process. Lett.*, vol. 27, pp. 241–245, Jan. 2020.
- [53] A. Conti, M. Guerra, D. Dardari, N. Decarli, and M. Z. Win, "Network Experimentation for Cooperative Localization," *IEEE J. Sel. Areas Commun.*, vol. 30, no. 2, pp. 467–475, Feb. 2012.
- [54] T. N. Nguyen, "Development of wireless sensor network to detect lameness in dairy cows," Ph.D. dissertation, Massachusetts Institute of Technology, 2022.
- [55] T. G. H. Ltd. (2018, May.) Specification of GW.11.A153. [Online]. Available: <https://cdn.taoglas.com/datasheets/{GW.11.A153}.pdf>
- [56] H. A. Sturges, "The choice of a class interval," *Journal of the american statistical association*, vol. 21, no. 153, pp. 65–66, 1926.
- [57] D. W. Scott, "Sturges' rule," *Wiley Interdisciplinary Reviews: Computational Statistics*, vol. 1, no. 3, pp. 303–306, 2009.

This figure "fig1.png" is available in "png" format from:

<http://arxiv.org/ps/2406.14664v1>